OPEN ACCESS

CrossMark

A Population of Short-duration Gamma-Ray Bursts with Dwarf Host Galaxies

Anya E. Nugent[1] ⓘ, Wen-fai Fong[1] ⓘ, Cristian Castrejon[1] ⓘ, Joel Leja[2,3,4] ⓘ, Michael Zevin[1,5] ⓘ, and Alexander P. Ji[6,7] ⓘ

[1] Center for Interdisciplinary Exploration and Research in Astrophysics (CIERA) and Department of Physics and Astronomy, Northwestern University, Evanston, IL 60208, USA; anyanugent2023@u.northwestern.edu
[2] Department of Astronomy & Astrophysics, The Pennsylvania State University, University Park, PA 16802, USA
[3] Institute for Computational & Data Sciences, The Pennsylvania State University, University Park, PA 16802, USA
[4] Institute for Gravitation and the Cosmos, The Pennsylvania State University, University Park, PA 16802, USA
[5] The Adler Planetarium, 1300 South DuSable Lake Shore Drive, Chicago, IL 60605, USA
[6] Department of Astronomy & Astrophysics, The University of Chicago, 5640 South Ellis Avenue, Chicago, IL 60637, USA
[7] Kavli Institute for Cosmological Physics, The University of Chicago, 5640 South Ellis Avenue, Chicago, IL 60637, USA

Abstract

We present a population of 11 of the faintest (>25.5 AB mag) short gamma-ray burst (GRB) host galaxies. We model their sparse available observations using the stellar population inference code Prospector-β and develop a novel implementation to incorporate the galaxy mass–radius relation. Assuming these hosts are randomly drawn from the galaxy population and conditioning this draw on their observed flux and size in a few photometric bands, we determine that these hosts have dwarf galaxy stellar masses of $7.0 \lesssim \log(M_*/M_\odot) \lesssim 9.1$. This is striking as only 14% of short GRB hosts with previous inferred stellar masses had $M_* \lesssim 10^9 M_\odot$. We further show these short GRBs have smaller physical and host-normalized offsets than the rest of the population, suggesting that the majority of their neutron star (NS) merger progenitors were retained within their hosts. The presumably shallow potentials of these hosts translate to small escape velocities of ∼5.5–80 km s^{-1}, indicative of either low postsupernova systemic velocities or short inspiral times. While short GRBs with identified dwarf host galaxies now comprise ≈14% of the total Swift-detected population, a number are likely missing in the current population, as larger systemic velocities (observed from the Galactic NS population) would result in highly offset short GRBs and less secure host associations. However, the revelation of a population of short GRBs retained in low-mass host galaxies offers a natural explanation for the observed r-process enrichment via NS mergers in Local Group dwarf galaxies, and has implications for gravitational-wave follow-up strategies.

Unified Astronomy Thesaurus concepts: Gravitational wave sources (677); Gamma-ray bursts (629); Dwarf galaxies (416)

1. Introduction

The astrophysical sites of heavy r-process element ($A > 130$) production have implications for the chemical enrichment and evolution of the Universe. Currently, the only observed production sites for r-process elements are neutron star (NS) mergers (Chornock et al. 2017; Kasen et al. 2017; McCully et al. 2017; Pian et al. 2017; Shappee et al. 2017; Tanvir et al. 2017). However, while the first NS merger, gravitational wave GW 170817, was discovered in an old, massive, and quiescent host galaxy (Blanchard et al. 2017; Levan et al. 2017; Palmese et al. 2017; Kilpatrick et al. 2022), evidence for r-process elements has also been discovered in different types of environments, including nearby low-metallicity dwarf galaxies and Galactic metal-poor stars (Eichler et al. 1989; McWilliam et al. 1995; Shetrone et al. 2001; Venn et al. 2012; Ji et al. 2016a; Côté et al. 2018; Hotokezaka et al. 2018). The abundances in these latter environments are challenging to explain with NS mergers alone. In particular, the occurrence rates of NS binaries may be too low to create all r-process abundances especially at low metallicity (Argast et al. 2004; Tsujimoto et al. 2015) and the expected delay times for the majority of NS mergers are too long for significant contributions in these young environments (Argast et al. 2004; Dominik et al. 2012; Wehmeyer et al. 2015;

Andrews & Mandel 2019; Zevin et al. 2022). Rather, supernovae (SNe) and collapsars (MacFadyen & Woosley 1999), which can occur on rapid timescales (stellar evolutionary timescales of ≲few megayears) with higher occurrence rates in low-metallicity environments have been used to explain the abundances (Qian 2000; Argast et al. 2004; Tsujimoto et al. 2015; Siegel et al. 2019; Skúladóttir et al. 2019; Brauer et al. 2021), although there is still no observational evidence that they produce r-process elements (Blanchard et al. 2023).

Despite support for a faster channel than NS mergers to explain the r-process elements in some dwarf galaxies, one such environment may have indeed been enriched from an NS merger event: the ∼$10^4 M_\odot$, low-metallicity Local Group dwarf galaxy Reticulum II. This dwarf galaxy exhibits r-process enrichment in several of its brightest stars (Ji et al. 2016a, 2016b) with yields suggestive of being derived from a single NS merger event, rather than a normal core-collapse supernova (CCSN; Beniamini et al. 2016; Safarzadeh & Scannapieco 2017; Ojima et al. 2018; Safarzadeh et al. 2019; Tarumi et al. 2020; Cowan et al. 2021; Jeon et al. 2021; Molero et al. 2021), although theoretical models of collapsars with large r-process yields have also been used to explain the abundances (Siegel et al. 2019). Additionally, evidence for delayed r-process production has been discovered in more massive dwarf galaxies or tidally disrupted dwarf galaxies (≈10^5–$10^9 M_\odot$; e.g., the LMC, Ursa Minor, Gaia–Sausage–Enceladus, and Wukong), with NS mergers being the most probable cause (e.g., Duggan et al. 2018; Matsuno et al. 2021;

Molero et al. 2021; Reggiani et al. 2021; Naidu et al. 2022; Limberg et al. 2023). If an NS merger was responsible for the r-process production in some of these dwarf galaxies, it is natural to search for direct evidence of NS mergers in low-mass galaxies.

Short-duration gamma-ray bursts (GRBs) offer a promising route as the majority are likely spawned from NS mergers (Abbott et al. 2017a; Goldstein et al. 2017; Savchenko et al. 2017), and they are routinely observed over a range of cosmological distances ($0.01 \lesssim z \lesssim 3.0$; Berger 2014; Selsing et al. 2018; Paterson et al. 2020; Fong et al. 2022; Nugent et al. 2022; O'Connor et al. 2022). However, despite the $\gtrsim 150$ short GRBs detected with NASA's Neil Gehrels Swift Observatory (Swift; Gehrels et al. 2004) and the 84 events with robust host galaxy associations (Fox et al. 2005; Villasenor et al. 2005; Berger et al. 2007; D'Avanzo et al. 2009; Fong et al. 2013; Berger 2014; De Pasquale 2019; Fong et al. 2022; O'Connor et al. 2022), there is an apparent lack of galaxies at stellar masses of $\lesssim 10^8 \, M_\odot$, and only $\approx 14\%$ of all Swift short GRBs are have stellar masses of $\lesssim 10^9 \, M_\odot$ (Nugent et al. 2022). Instead, short GRB hosts generally trace the luminosities, star formation rates (SFRs), and metallicities of the typical star-forming field galaxy population, with $\approx 15\%$ in less active galaxies (Leibler & Berger 2010; Nugent et al. 2022). On the other hand, the host galaxies of long-duration GRBs and CCSNe, which originate from massive stars, are comprised of $\approx 35\%$ dwarfs (Schulze et al. 2021; Taggart & Perley 2021).

Given the strong enrichment of r-process elements in Reticulum II, this additionally requires an NS binary to have small NS natal kicks ($\lesssim 15$ km s^{-1}; Beniamini et al. 2016; Bramante & Linden 2016) to be retained in the dwarf-galaxy center and not overcome its relatively small escape velocity. This, however, is contradictory to the larger galactocentric offsets of short GRBs (≈ 5.6–7.7 kpc; Church et al. 2011; Fong & Berger 2013; Tunnicliffe et al. 2014; Fong et al. 2022; O'Connor et al. 2022), which likely have progenitors with larger natal kicks (see Zevin et al. 2020; Perets & Beniamini 2021). Furthermore, inferences on the delays of star formation episodes in dwarf galaxies (Bland-Hawthorn et al. 2015; Ji et al. 2015, 2023) suggest that the r-process–producing event in Reticulum II likely has a delay time of $\lesssim 100$ Myr, at odds with the inferred minimum delay times from host stellar populations of ≈ 200 Myr (Nakar et al. 2006; Berger et al. 2007; Jeong & Lee 2010; Hao & Yuan 2013; Wanderman & Piran 2015; Anand et al. 2018; Zevin et al. 2022) and the observed population of Galactic binary NS (BNS) systems (Tauris et al. 2017; Andrews & Mandel 2019). However, predictions made from stellar population synthesis and models of the delay time distribution of Galactic BNS systems estimate that the minimum delay time can be as low as ~ 10 Myr (Belczynski et al. 2002; Dominik et al. 2012; Vigna-Gómez et al. 2018; Beniamini & Piran 2019).

Current short GRB host samples are generally limited to galaxies with luminosities $\gtrsim 10^9 \, L_\odot$ especially beyond $z \gtrsim 1$ (e.g., Fong et al. 2022; O'Connor et al. 2022) and it has been challenging to overcome the bias against identifying high-redshift ($z \gtrsim 1.5$) and/or low-luminosity hosts. To fill this gap and explore a possible missing dwarf host population, here we present modeling of 11 faint short GRB hosts ($\gtrsim 25.5$ mag) that have been absent in previous stellar population modeling studies, to estimate their redshifts and stellar masses. By default, these hosts have limited observational data, requiring

novel stellar population modeling techniques in order to put useful constraints on their properties. This sample represents all remaining short GRBs with robust host associations that do not have previous stellar population modeling results, but for which it is possible with novel stellar population modeling techniques. We discuss our host sample and the available observations in Section 2. In Sections 3–4, we detail our stellar population modeling and results. In Section 5, we examine any trends with respect to short GRB properties, including the gamma-ray properties, afterglow luminosities, and galacto-centric offsets. We discuss selection effects, delay times, and implications for this population and GW follow-up in Section 6. Finally, we summarize our main conclusions in Section 7.

Unless otherwise stated, all observations are reported in the AB magnitude system and have been corrected for Galactic extinction in the direction of the GRB (Cardelli et al. 1989; Schlafly & Finkbeiner 2011). We employ a standard WMAP9 cosmology of $H_0 = 69.6$ km s^{-1} Mpc^{-1}, $\Omega_M = 0.286$, and $\Omega_{\rm vac} = 0.714$ (Hinshaw et al. 2013; Bennett et al. 2014).

2. Host Sample and Observations

We start with the host sample described in Fong et al. (2022), which includes host galaxy associations for 84 short GRBs discovered by Swift with afterglows detected to $\lesssim 5''$ localization and not along high Galactic extinction sight lines ($A_V < 2$ mag) that would impair possible host detection. While 69 hosts had sufficient data to be modeled in Nugent et al. (2022), there are 14 remaining that do not have determined stellar population properties. Of these, 11 comprise the faintest detected hosts in the entire sample, with optical and near-infrared magnitudes $\gtrsim 25.5$ (only four other hosts from the parent sample of 69 have comparable optical magnitudes, but with determined photometric redshifts). These 11 hosts, listed in Table 1, are almost exclusively detected with NASA's Hubble Space Telescope (HST) in only one or two photometric filters and constitute the host sample in this work. Of the three hosts not included in our sample, one is a low-redshift GRB in a crowded field (GRB 080905A) and the other two (GRBs 081226A and 160601A) do not have HST observations for effective radii measurements, which are used in this analysis (see Section 3.2).

According to Fong et al. (2022), the majority of hosts in this faint sample are classified as "Gold" host associations (probability of chance coincidence, $P_{\rm cc} < 0.02$), with three hosts as "Silver" (GRBs 080503, 131004A, and 150424A; $0.02 < P_{\rm cc} < 0.09$), and two as "Bronze" (GRBs 091109B and 130912A; $0.09 < P_{\rm cc} < 0.20$). We list the association type in Table 1. Two of the hosts, furthermore, have spectroscopic redshifts determined from their GRB afterglows: GRB 090426A ($z = 2.609$) and GRB 131004A ($z = 0.717$), but undetermined stellar masses. For the remaining nine host galaxies, we determine upper limits on the redshifts from the optical afterglow detections (available for all GRBs except GRB 211106A), corresponding to a lack of suppression blue-ward of the Lyα limit (Fong et al. 2015). This effectively places upper limits on their redshifts of $z \approx 1$–4 depending on the burst. For GRB 150424A, Jin et al. (2018) report a probable photometric redshift from the host spectral energy distribution (SED) of $z \approx 1.2$, while Knust et al. (2017) determine the redshift is likely $z \approx 1.0$ from GRB afterglow properties, which are both very close or greater than the maximum possible

Table 1
Host Galaxy Observations

GRB	R.A.	Decl.	Sample	Redshift or Limit	Filter	AB Mag	r_e (arcsec)	References
060121	$09^h09^m52^s.026$	$+45°39'45''.538$	Gold	<4.1	F606W	27.48 ± 0.32	0.36	(1, 2)
060313	$04^h26^m28^s.402$	$-10°50'39''.901$	Gold	<1.1	F475W	26.89 ± 0.20	0.10	(1, 2)
					F775W	26.31 ± 0.18		(1, 2)
070707	$17^h50^m58^s.555$	$-68°55'27''.6$	Gold	<3.6	F606W	26.86 ± 0.12	0.36	(3)
					F160W	26.04 ± 0.24		(3)
080503	$19^h06^m28^s.901$	$+68°47'34''.78$	Silver	<4.2	F606W	27.15 ± 0.20	0.26	(4)
					F160W	26.57 ± 0.06		(1, 3)
					$3.6\mu m$	>23.97		(6)
					$4.5\mu m$	>23.55		(6)
090305A	$16^h07^m07^s.596$	$-31°33'22''.53$	Gold	<2.9	F160W	25.29 ± 0.10	0.36	(3)
090426A	$12^h36^m18^s.047$	$+32°59'09''.46$	Gold	2.609	F160W	25.57 ± 0.07	0.21	(3)
					$3.6\mu m$	>24.58		(6)
091109B	$07^h30^m56^s.55$	$-54°05'23''.22$	Bronze	<4.4	F110W	27.81 ± 0.24	0.27	(6)
130912A	$03^h10^m22^s.2$	$+13°59'48''.74$	Bronze	<4.1	F110W	27.47 ± 0.23	0.34	(6)
131004A	$19^h44^m27^s.064$	$-02°57'30''.429$	Silver	0.717	F110W	25.46 ± 0.09	0.44	(6)
150424A	$10^h09^m13^s.406$	$-26°37'51''.745$	Silver	<2.0	F105W	26.26 ± 0.20	0.28	(5)
					F125W	26.29 ± 0.15		(6)
					F160W	25.89 ± 0.14		(6)
					$3.6\mu m$	>23.35		(6)
211106A	$22^h54^m20^s.541$	$-53°13'50''.548$	Gold	...	V	25.45 ± 0.08	0.20	(7)
					R	26.53 ± 0.23		(7)
					F814W	25.79 ± 0.07		(6)
					F110W	25.71 ± 0.02		(6)

Note. The localizations, sample (confidence of host association), spectroscopic redshifts (if it is known) or maximum possible redshift of the GRB, available HST and Very Large Telescope (VLT; MUSE V band and FORS2 R band) detections, Spitzer upper limits, and the effective radii (r_e) of the short GRB hosts studied in this work. Magnitudes are uncorrected for Galactic extinction in the direction of the host.
References: (1) This work; (2) Fong et al. (2010); (3) Fong & Berger (2013); (4) Perley et al. (2009); (5) Jin et al. (2018); (6) Fong et al. (2022); and (7) Ferro et al. (2023).

redshift from the Lyα limit ($z < 1.1$). Thus, given the conflicting analyses from the literature and the fairly strict limit from Lyα for this burst, we set the maximum redshift of GRB 150424A to $z < 2.0$ to be conservative.

In Figure 1, we show the near-infrared luminosities of the faint host galaxies as a function of redshift, compared to the population with previously determined stellar population properties (Nugent et al. 2022). For the latter sample, in the absence of relevant near-infrared data, we use the model SEDs derived in Nugent et al. (2022) to derive a J-band magnitude. We note that these faint hosts represent the lowest-luminosity host galaxies to date and stand in contrast to the rest of the host population, out to a maximum redshift $z \approx 4$, where they begin to appear more similar to the current host sample ($\log(L_{NIR}/L_\odot) \approx 10.1$). As near-infrared luminosities are strongly correlated to stellar mass, this hints that unless they are all at high redshift, they likely have smaller stellar masses as well.

We collect HST and VLT photometry and upper limits from NASA's Spitzer Space Telescope in Fong et al. (2010), Fong & Berger (2013), Fong et al. (2022), and Ferro et al. (2023). We also include two new photometric detections for the host of GRB 211106A (Ferro et al. 2023) and one additional photometric detection for GRB 150424A in Jin et al. (2018). For GRBs 060121, 060313, and 080503 (only F160W filter), we perform aperture photometry using standard tasks in IRAF/ `phot`, whereas such measurements are available for the other hosts in our sample. We further collect the effective radii (r_e) from Fong et al. (2022), which are available for all of the host
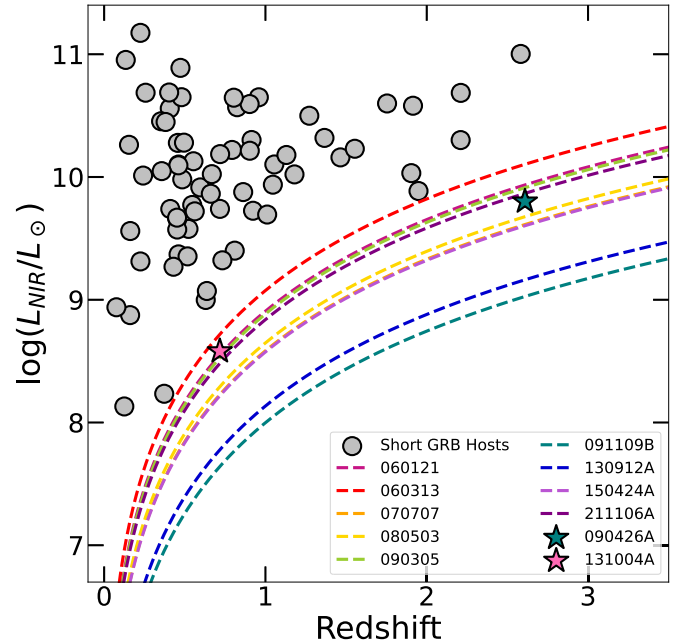

Figure 1. The observed or inferred J-band luminosities and redshifts of the sample of short GRB host galaxies studied in Nugent et al. (2022; gray circles). We plot the observed luminosities for the faint short GRB host sample in Table 1, using either the F110W filter or the filter closest to the J-band central wavelength for each short GRB. Dashed lines represent the nine hosts with no known redshifts and stars represent the hosts with known redshifts. We see that the faint host sample is generally less luminous across all redshift than the rest of the host sample, implying they likely represent a unique group of low-luminosity, low-mass environments.
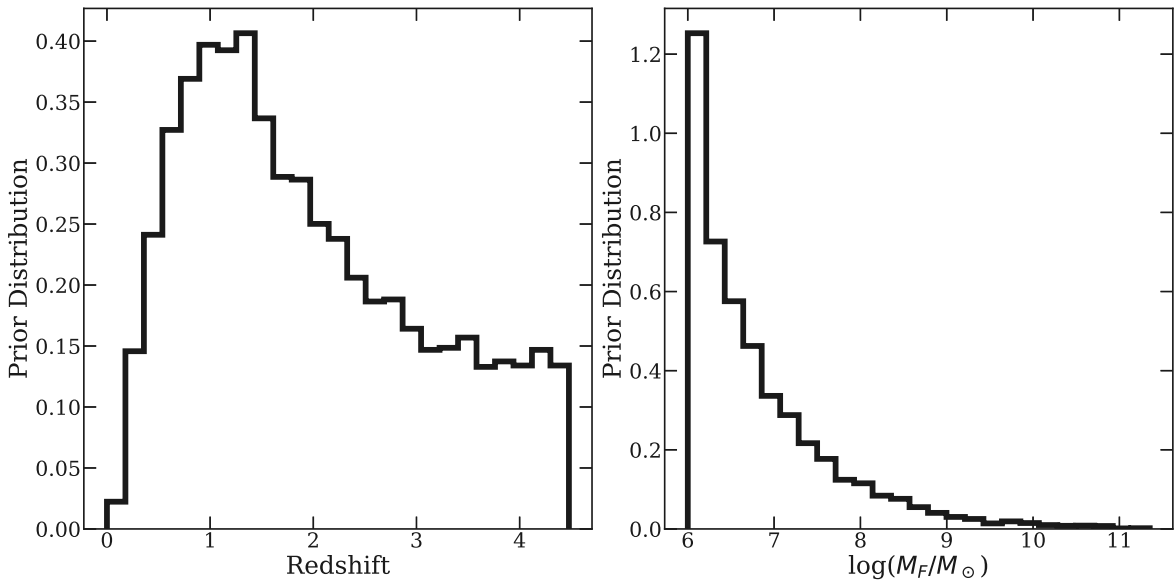
Figure 2. The `Prospector-β` priors on redshift (z) and mass formed (M_F) (Wang et al. 2023a). The nonuniform priors better predict the stellar population properties of faint galaxy targets with limited photometric coverage, as they limit the sampling to only plausible solutions based on observed galaxy trends.

galaxies in our sample. All photometry, spectroscopic redshifts (when available), maximum possible redshifts, and r_e measurements are listed in Table 1.

3. Stellar Population Modeling

3.1. Prospector-β

To model the stellar population properties of the host galaxies, we use the Python-based SED code `Prospector-β` (Wang et al. 2023a) over all photometric detections and upper limits of the hosts. `Prospector-β` was specifically designed to infer the redshifts and stellar masses of faint galaxies with limited photometric wavelength coverage, and thus far has been used on faint HST and James Webb Space Telescope (JWST) targets (Wang et al. 2023b). In contrast to other versions of `Prospector` (Leja et al. 2019; Johnson et al. 2021), it uses nonuniform priors on key stellar population properties, including mass formed (M_F), redshift (z), stellar metallicity (Z_*), and the star formation history (SFH), informed from mock catalogs and observations (Williams et al. 2018; Leja et al. 2020), which greatly reduce the parameter space to only stellar population property solutions that are consistent with observed galaxy populations in deep extragalactic fields. Indeed, it has already been shown that the `Prospector-β` nonuniform priors better estimate the stellar masses of mock galaxies with limited photometric data than uniform priors (Wang et al. 2023a). With limited observational data (the majority with ⩽ two data points each), our sample of 11 faint short GRB hosts represents an excellent test data set for `Prospector-β`. However, while `Prospector-β` can give robust estimates on redshift and stellar mass with very few photometric detections, it is not expected to constrain Z_* and the SFH, as these are best determined through modeling the shape of an SED across a wide range of wavelengths. These are nonetheless included in the fits, not in the hopes of producing useful constraints on them, but rather in order to marginalize over them properly. `Prospector-β` fits the observed photometry of a galaxy to model SEDs produced through `FSPS` and `python-fsps` (Conroy et al. 2009;

Conroy & Gunn 2010), which, by default, use `MIST` models (Paxton et al. 2018) and the `MILES` spectral library (Falcón-Barroso et al. 2011). We apply the nested-sampling fitting routine `dynesty` to derive posterior distributions of the stellar population properties of interest, including M_F, z (when it is not already known), Z_*, and the SFH.

`Prospector-β` contains several different model templates, which have various combinations of prior distributions. For the faint hosts with no known redshifts, we use the `NzSFH` model template. The `NzSFH` template employs a redshift prior that is based on the number density of galaxies across $0 \leqslant z \leqslant 15$, given by Equation (2) in Wang et al. (2023a), and shown in Figure 2. We modify the redshift prior by placing a maximum given by the detection of the optical afterglow for each short GRB (Table 1). We set the maximum redshift for GRB 211106A to $z = 4.5$ as this GRB has no detected optical afterglow and we do not expect short GRBs to be detected by Swift much greater than this redshift (Lien et al. 2016). The M_F prior in the `NzSFH` template is dependent on the mass function derived in Leja et al. (2020) at a given redshift z and has range $10^6 \leqslant M_F \leqslant 10^{12}$ $M_\odot$ (shown in Figure 2). We note that the mass function in Leja et al. (2020) is only constrained down to $\approx 10^8$ $M_\odot$, depending on the redshift. Thus, the function is extrapolated down to lower stellar masses. As there are relatively more lower-mass galaxies in the Universe than higher-mass galaxies, the prior tends to favor lower-mass solutions, although it does not forbid exotic parameter spaces given sufficiently convincing data; for example, it has been used to make recent discoveries with JWST of high-mass galaxies at higher redshifts (Labbé et al. 2023). We note that M_F is converted to stellar mass M_* within the `Prospector` infrastructure, which we report hereafter. The `NzSFH` template furthermore includes a Gaussian prior on Z_*, which is dependent on the mass–metallicity relation described in Gallazzi et al. (2005). It also incorporates a nonparametric SFH that is a function of the age of the Universe at redshift z and the mass formed in the galaxy. We fit for the SFR in seven log-spaced age bins to determine the SFH; we refer the reader to a thorough description of the dynamic nonparametric SFH

prior and an explanation for how the age bins are made in Wang et al. (2023a). Finally, we apply the Kriek & Conroy (2013) dust attenuation model which measures the offset from the Calzetti et al. (2000) attenuation curve and the ratio of dust attenuated from old to young stellar light, as this is the standard dust model in Prospector-β. For the two faint short GRB hosts that have known redshifts, we employ the PhiSFHz-fixed model templates, which contain prior distributions in M_F, Z_*, and the SFH that are identical to those in the NzSFH template, but allow redshift to be a fixed parameter.

3.2. Implementation of the Mass–Radius Relation

By default, we have limited available data for our sample of faint short GRB hosts, making them excellent cases for modeling with Prospector-β. Notably, stellar mass and redshift can be robustly constrained in some cases even in the absence of extensive photometric coverage (Akins et al. 2023), if the targets do not have unusual colors or magnitudes given their properties and redshifts. However, given the lack of observational data for this sample of hosts, we wish to expand upon the current Prospector-β infrastructure to find more informed constraints on the true stellar masses and redshifts using the well-known and characterized galaxy mass–radius relation (van der Wel et al. 2014). By modifying Prospector-β to be informed by the galaxy size, in addition to the integrated flux, we can better constrain the stellar mass estimates to more physical values. We note that while this is a novel implementation in Prospector-β, this concept has been tested previously and successfully in Dey et al. (2022).

We employ the van der Wel et al. (2014) mass–radius relation in our analysis. This relation specifically constrains the stellar mass of a galaxy given its physical effective radius (radius from within which half of the galaxy light is contained; r_e), or vice versa, at a given redshift and is based on galaxies observed in the CANDELS/3D-HST (Koekemoer et al. 2011; Brammer et al. 2012) fields with HST/WFC3 across $0 < z < 3$. The stellar masses of these galaxies were determined with the stellar population synthesis code FAST (Kriek et al. 2009) and the r_e values were calculated using GALFIT (Häussler et al. 2007) over the available HST/WFC3 data (F814W, F125W, F140W, and F160W filters; van der Wel et al. 2012).[8] Although the stellar masses derived from FAST are known to be ≈0.1–0.2 dex smaller than the stellar masses inferred from Prospector (Leja et al. 2019), the scatter on the mass–radius relation, which we take into account in our modeling, is the dominant source of uncertainty and outweighs this small systematic offset.

We describe our novel implementation of the van der Wel et al. (2014) mass–radius relation in Prospector-β in the Appendix. In essence, we use the observed size (see Table 1; Fong et al. 2010; Fong & Berger 2013; Fong et al. 2022) and photometry of the host to constrain the stellar population properties, as opposed to just the photometry (Section 3.1). We do so by determining the likelihood of a host r_e within a distribution of possible galaxy sizes derived at a sampled Prospector-β stellar mass and redshift in the nested-sampling routine. Hereafter, we call the Prospector-β and mass–radius relation method Prospector-β (M_*–r_e).

---

[8] We note that the van der Wel et al. (2014) mass–radius relation was observed for galaxies down to $M_* \approx 10^9 \, M_\odot$. However, it has been shown that this function can be reasonably extrapolated down to lower stellar masses (Nedkova et al. 2021), especially for late-type galaxies.

The inclusion of the van der Wel et al. (2014) mass–radius relation effectively increases the probability of Prospector-β samples where the observed size of the galaxy is well constrained within a distribution of physical sizes from M_* and z. These probabilities are maximized when the observed galaxy size is closer to the mean of the physical size distribution, rather than on the outskirts. As the uncertainty on the van der Wel et al. (2014) mass–radius relation increases with redshift, solutions at lower redshifts that are in good agreement with the observed size are likely to be maximized more so than solutions at high redshift, where the observed size is further from the mean of the distribution derived from the sampled M_* and z. This approach implicitly assumes that GRB hosts are typical members of the galaxy population and if they instead only occur in highly unusual systems, the constraints will be more difficult to interpret. However, given that we have already seen that short GRB hosts do have similar luminosities, SFRs, stellar masses, and metallicities to field galaxy populations (Fong et al. 2022; Nugent et al. 2022; O'Connor et al. 2022), we find that this underlying assumption is likely legitimate.

4. Host Galaxy Properties

4.1. Stellar Population Modeling Results

Here we present and compare the results of the stellar population fitting from both Prospector-β and Prospector-β (M_*–r_e); we list the redshift and stellar mass medians and 68% confidence intervals from these fits in Table 2 and show the posterior distributions of the nine hosts without previously known redshifts in Figure 3. First, when comparing the Prospector-β–determined posterior distributions in stellar mass and redshift to the prior distributions (see Figure 2), we find that with the exception of GRB 060121, all posterior distributions are distinct from the prior distributions, suggesting that the data are providing meaningful constraints and the posteriors are not simply tracing the prior. Since GRB 060121 is one of the faintest in the sample, it is somewhat unsurprising that the data may not be sufficient to provide strong deviations from the prior.

For the Prospector-β–modeled population, we find a redshift median and 68% confidence interval on the population of $z = 0.73^{+1.36}_{-0.31}$ and stellar mass median and 68% confidence interval of $\log(M_*/M_\odot) = 7.97^{+1.02}_{-0.84}$. While the redshifts are comparable to those found for the short GRB population (Fong et al. 2022; Nugent et al. 2022), the stellar masses for the faint host population are lower than the rest of the observed host population, which have a median and 68% confidence interval of $\log(M_*/M_\odot) = 9.69^{+0.75}_{-0.65}$ (Nugent et al. 2022).

For the Prospector-β (M_*–r_e) fits, we find that slightly lower redshifts are preferred (the median and 68% confidence interval decrease to $z = 0.54^{+0.52}_{-0.29}$). The stellar masses remain fairly consistent with the original fits, with a median and 68% confidence interval of $\log(M_*/M_\odot) = 7.79^{+1.22}_{-0.84}$, although still lower than the rest of the short GRB population. Comparing the results of the Prospector-β and Prospector-β (M_*–r_e) fits (Figure 3), we note that while the majority of results shift toward lower-redshift solutions, the stellar masses stay consistent within the 68% confidence intervals. Given that the majority of this population falls at $M_* \lesssim 10^9 \, M_\odot$, the stellar mass limit of dwarf galaxies (Bullock & Boylan-Kolchin 2017), these results strongly suggest that this is a population of dwarf galaxies. Indeed, ≈84% of the Prospector-β (M_*–r_e)

Table 2
Stellar Population Modeling Results

GRB	Prospector-β			Prospector-β (M_*–r_e)		
	z	$\log(M_*/M_\odot)$	r_e (kpc)	z	$\log(M_*/M_\odot)$	r_e (kpc)
060121	$1.19^{+1.4}_{-0.69}$	$6.94^{+1.44}_{-0.91}$	$2.87^{+0.22}_{-0.63}$	$0.43^{+0.52}_{-0.24}$	$8.31^{+0.91}_{-0.96}$	$2.06^{+0.82}_{-0.88}$
060313	$0.49^{+0.42}_{-0.24}$	$7.42^{+0.58}_{-0.52}$	$0.61^{+0.18}_{-0.22}$	$0.64^{+0.28}_{-0.32}$	$7.36^{+0.53}_{-0.54}$	$0.7^{+0.1}_{-0.22}$
070707	$0.73^{+1.01}_{-0.4}$	$7.75^{+0.56}_{-0.64}$	$2.65^{+0.39}_{-0.93}$	$0.29^{+0.25}_{-0.11}$	$7.23^{+0.59}_{-0.45}$	$1.6^{+0.73}_{-0.48}$
080503	$1.05^{+1.65}_{-0.75}$	$7.73^{+0.74}_{-0.68}$	$2.01^{+0.2}_{-0.86}$	$0.41^{+0.4}_{-0.19}$	$7.01^{+0.75}_{-0.4}$	$1.43^{+0.53}_{-0.51}$
090305	$0.81^{+0.59}_{-0.39}$	$8.63^{+0.6}_{-0.63}$	$2.77^{+0.29}_{-0.73}$	$0.58^{+0.54}_{-0.31}$	$8.34^{+0.85}_{-0.74}$	$2.41^{+0.59}_{-0.89}$
090426A	2.609	$9.11^{+0.33}_{-0.4}$	1.72	2.609	$9.11^{+0.3}_{-0.39}$	1.72
091109B	$0.82^{+0.69}_{-0.46}$	$7.63^{+0.92}_{-0.82}$	$2.06^{+0.25}_{-0.68}$	$0.48^{+0.47}_{-0.22}$	$7.32^{+0.95}_{-0.69}$	$1.64^{+0.5}_{-0.53}$
130912A	$0.81^{+0.58}_{-0.42}$	$7.82^{+0.86}_{-0.75}$	$2.59^{+0.3}_{-0.76}$	$0.32^{+0.52}_{-0.14}$	$7.28^{+1.26}_{-0.71}$	$1.61^{+1.01}_{-0.57}$
131004A	0.717	$9.07^{+0.54}_{-0.53}$	3.23	0.717	$9.05^{+0.38}_{-0.36}$	3.23
150424A	$0.61^{+0.57}_{-0.3}$	$7.89^{+0.5}_{-0.51}$	$1.92^{+0.44}_{-0.62}$	$0.54^{+0.46}_{-0.23}$	$7.78^{+0.56}_{-0.49}$	$1.81^{+0.47}_{-0.52}$
211106A	$0.73^{+0.02}_{-0.01}$	$7.88^{+0.5}_{-0.0}$	$1.47^{+0.0}_{-0.04}$	$0.45^{+0.32}_{-0.0}$	$6.98^{+1.21}_{-0.0}$	$1.16^{+0.34}_{-0.0}$

Note. The results in redshift, stellar mass, and effective radii (r_e) from stellar population modeling fits done with Prospector-β and Prospector-β (M_*–r_e) (e.g., with the van der Wel et al. 2014 mass–radius relation). For the r_e estimates, we convert the angular values in Table 1 to physical values in kiloparsecs using the redshift posterior distribution. We note that GRBs 090426A and 131004A have known spectroscopic redshifts via their afterglows.

posterior distributions across all 11 hosts result in $M_* \lesssim 10^9 M_\odot$. We further note that even when we only analyze the population of very robust host associations (Gold Sample; Table 1), the stellar mass stays similarly low, at $\log(M_*/M_\odot) = 7.76^{+1.28}_{-0.78}$, hinting that NS mergers are indeed occurring in low-mass environments.

4.2. Testing the Prospector-β Framework

To understand better the stellar mass and redshift results for our faint short GRB hosts, we perform Prospector-β and Prospector-β (M_*–r_e) fits, setting the redshift free for the two GRBs with known redshifts, GRBs 090426A and 131004A, and compare these results to the fixed redshift results (which represents the likely "true" results). In Figure 4, we show the posterior distributions of their redshifts and stellar masses for the Prospector-β fits and Prospector-β (M_*–r_e) fits and overplot the "true" results as black lines. We find that the true redshift for GRB 090426A ($z = 2.609$) lies near the 99th percentile of, but still within, the evolving galaxy population after conditioning on the observed flux and size, while the stellar mass is fairly consistent. This is an interesting result and may suggest that the host of this GRB has other unusual properties compared to the normal galaxy population. Though possibly counterintuitive, we also note that it is possible for the inferred stellar mass to stay consistent across a range of redshifts, as at higher redshifts, galaxy colors tend to be bluer, which decreases their mass-to-luminosity ratio, while their intrinsic luminosity is higher due to cosmological dimming. Subsequently, stellar mass estimates can stay flat over a range of redshifts. In the case of GRB 131004A, the true redshift ($z = 0.717$) and stellar mass estimate fall within the 68% confidence interval for both fits, suggesting this may be a more typical galaxy in terms of its photometric properties and size.

As an additional check, we also test our Prospector-β and Prospector-β (M_*–r_e) methods on 11 star-forming short GRB hosts in Fong et al. (2022) and Nugent et al. (2022) that have known redshifts and effective radii measurements to determine their estimated stellar masses in the scenario where their redshifts are unknown. These include the hosts of GRBs 051221A, 060614, 061006, 070429B, 070714B, 070724A, 071227A, 090510, 130603B, 160821B, and 200522A. We use all the

photometry for each of these hosts in Fong et al. (2022) and set their maximum redshift to $z = 3.0$, but otherwise use the same Prospector-β and Prospector-β (M_*–r_e) models as described in Section 3. We find a median stellar mass difference between the published stellar masses in Nugent et al. (2022) and those from our Prospector-β runs of $\Delta\log(M_*/M_\odot) \approx$ 0.4 dex. When we include the mass–radius relation, we find a slightly lower median difference of $\Delta\log(M_*/M_\odot) \approx 0.3$ dex. In either case, approximately half of the fits result in stellar masses greater than those that were previously published, and half are lower. Thus, while the test cases for GRBs 090426A and 131004A both lead to lower stellar mass estimates than when using their known redshifts, we see no evidence when using a larger population of short GRB hosts that there is a systematic bias in the Prospector-β or Prospector-β (M_*–r_e) methods toward lower stellar masses.

Taken together, these test cases all show that stellar mass is a fairly robust parameter, but redshift may be more challenging to constrain especially when a galaxy's properties deviate from the normal population. Given this insight, we emphasize that the dwarf host implication for the sample studied here is credible.

4.3. Comparison to the Full Short GRB Host Sample

We compare the redshifts and stellar masses of the faint host population to those of the entire short GRB host population in Figure 5. Strikingly, while the large majority of short GRB hosts have stellar masses of $M_* \gtrsim 10^9 M_\odot$, our entire sample falls near or below this value, regardless of the inclusion of the M_*–r_e relation; indeed, only 14% of the 69 hosts with stellar mass estimates in Nugent et al. (2022) have $\log(M_*/M_\odot) \lesssim 9$. Including our faint host population studied here in the stellar mass distribution of all short GRB hosts (to make a total of 80 modeled) does not significantly shift the population median, but extends the low-mass tail, as shown in Figure 6. We find that both the Prospector-β and Prospector-β (M_*–r_e) fits change the stellar mass median and 68% confidence interval of the entire short GRB host population to $\log(M_*/M_\odot) = 9.57^{+0.78}_{-1.02}$. Including the 10 hosts in Nugent et al. (2022) that can be classified as dwarf galaxies ($M_* \lesssim 10^9 M_\odot$; Bullock & Boylan-Kolchin 2017), we find that out of the population of
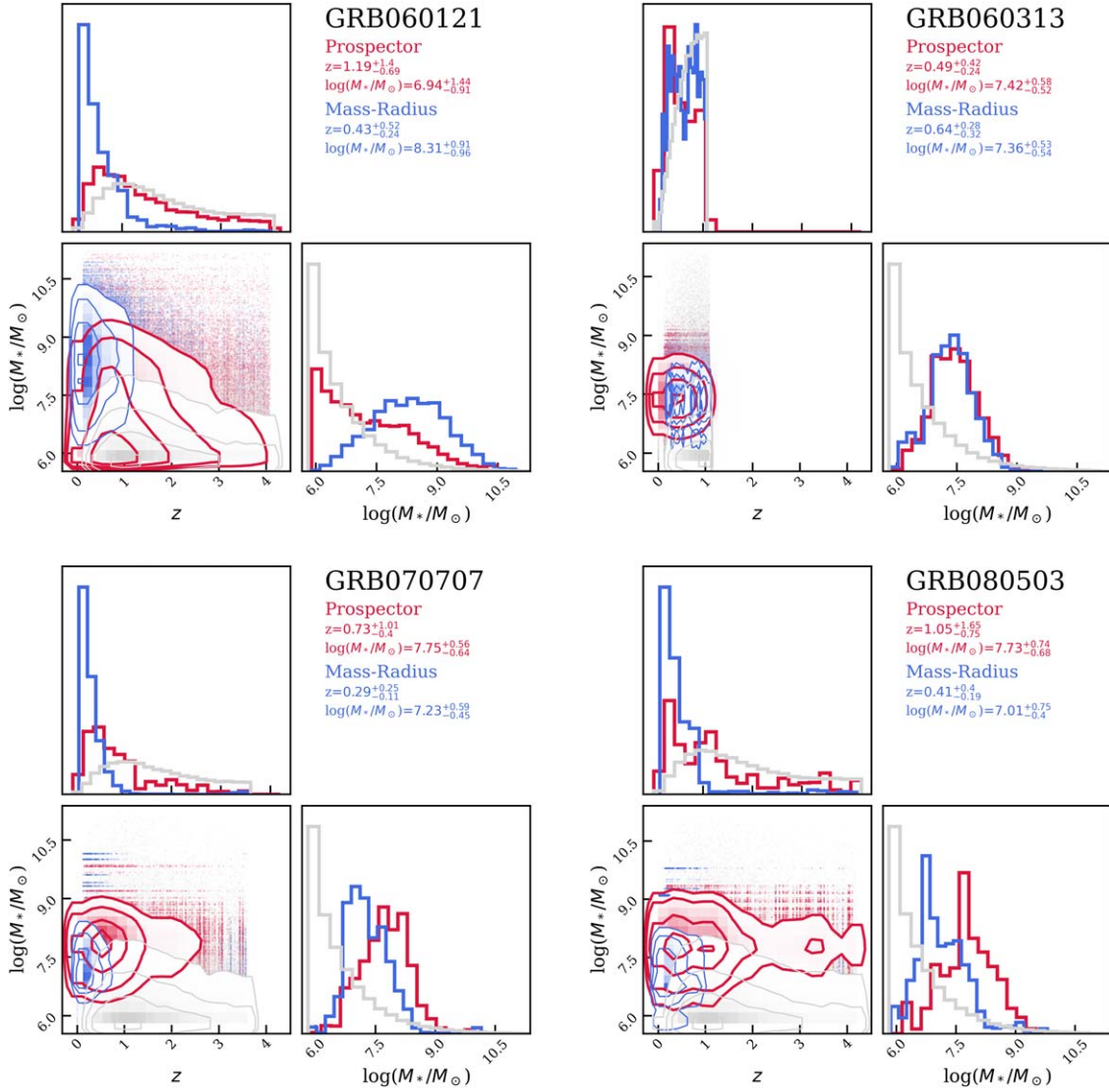
Figure 3. The original Prospector-β fits (red) compared to Prospector-β and mass–radius fits (blue) for the sample of nine faint short GRB hosts with no known redshifts. The prior distributions in stellar mass and redshift are shown in gray. We find that the addition of the mass–radius relation into the fits tends to lead to more constrained redshift and stellar mass estimates, with the majority of solutions leading to lower redshifts, while the stellar mass estimates stay fairly similar.

∼155 Swift short GRBs detected over 2005–2023 (Lien et al. 2016), ≈13.5% occur in dwarf galaxies (with ≈8% in galaxies with $M_* \lesssim 10^8 \, M_\odot$). We are likely missing some short GRBs in dwarf galaxies (see Section 6.1), so these percentages probably represent lower limits. In fact, the true fraction could in reality be more comparable to the population of field galaxies that have $M_* \lesssim 10^9 \, M_\odot$, which is ≈20% of the total galaxy population estimated from the Local Volume Legacy Survey (Lee et al. 2011; Taggart & Perley 2021).

Overall, our results show that these events very likely occurred in low-mass environments, and that the host galaxy population of short GRBs is more diverse than previously thought.

5. Short GRB Properties

5.1. Optical Afterglow Luminosities and Offsets

We next explore the properties of the faint host sample to determine if there are any other distinguishing features that set them apart from the rest of the short GRB host population. We

first compare their optical afterglow luminosities and galacto-centric offsets. As afterglow luminosity generally scales with circumburst density (Granot & Sari 2002), it can be used as a proxy for the burst environment. It was also found that short GRBs at larger offsets generally have fainter observed afterglows, again a likely by-product of decreasing interstellar medium (ISM) density at larger offsets (Perna & Belczynski 2002; Berger 2010). Thus, by exploring a combination of luminosity and offsets, we can probe the local properties of the faint host sample.

First, all short GRBs in the faint host sample have optical afterglow detections, except for GRB 211106A.[9] This is a much higher fraction of events with an optical afterglow detection than the full short GRB population (only ≈30%; Berger 2014; Fong et al. 2015). However, this is likely a product of how this sample was selected, as it becomes increasingly challenging to make host assignments for

---

[9] This event had both bright millimeter and radio detections, and a possible explanation for its optical darkness is the high dust extinction surrounding the event (Laskar et al. 2022; Ferro et al. 2023).
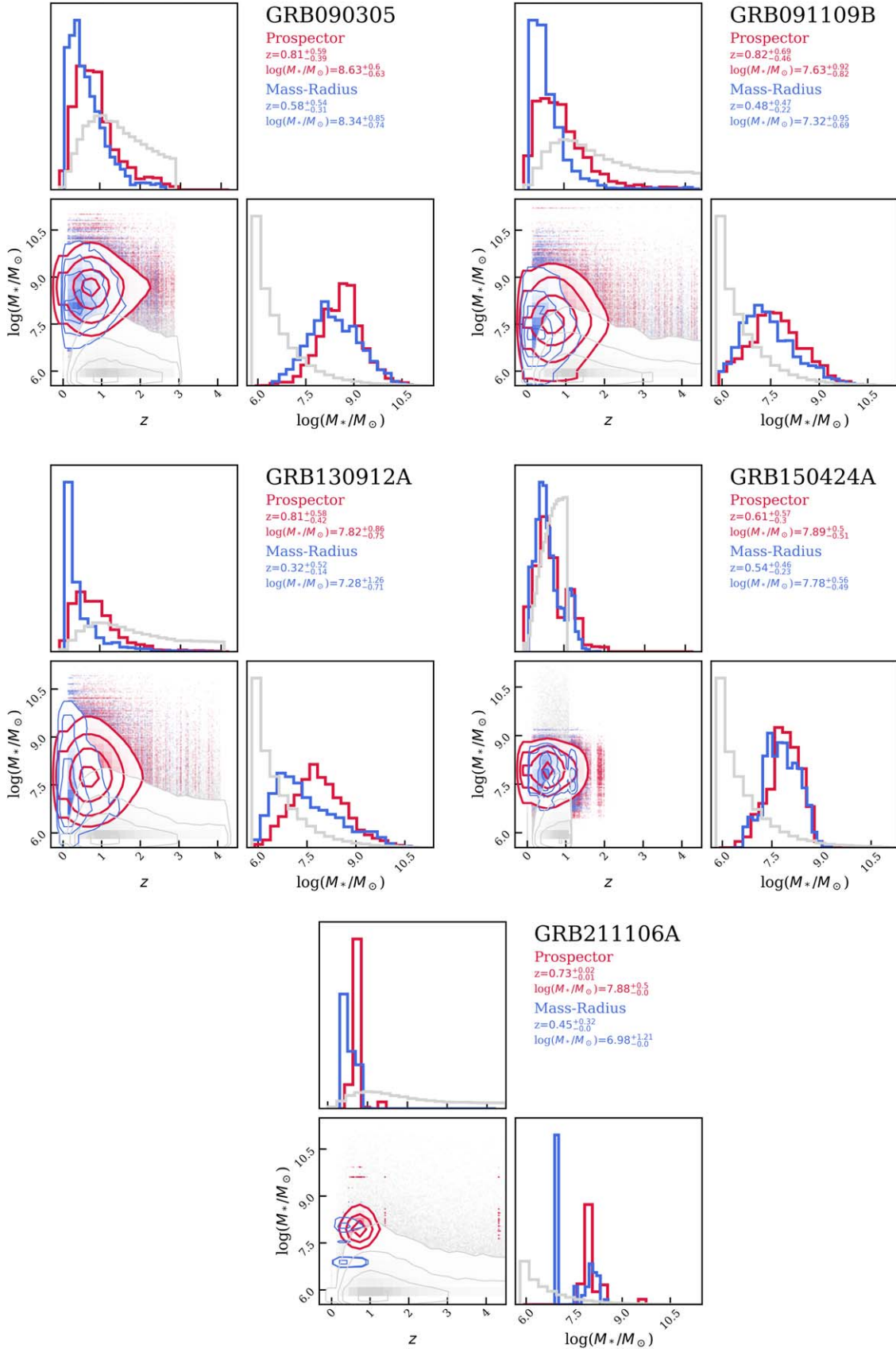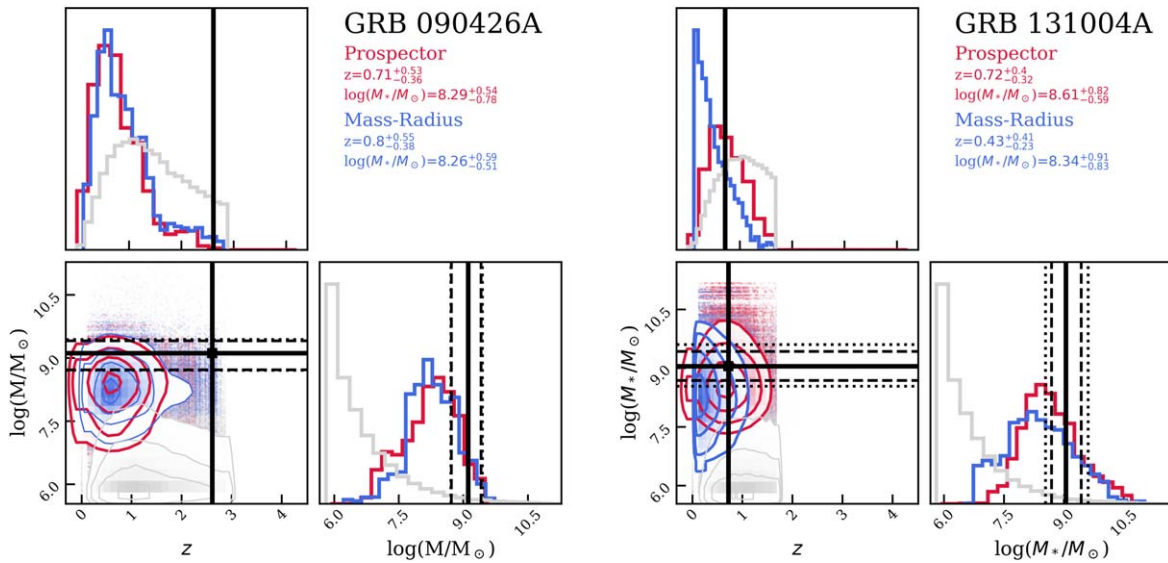
Figure 3. (Continued.)

Figure 4. The stellar mass and redshift estimate results for the `Prospector-β` (red) and `Prospector-β` ($M_*–r_e$) (blue) test cases for the two faint hosts with known redshifts: GRBs 090426A (left) and 131004A (right). The prior distributions are shown in gray. We plot the medians of their stellar mass estimates from the fits using their known redshifts (black line), along with the 68% confidence regions for the `Prospector-β` fit (dashed black lines) and the `Prospector-β` ($M_*–r_e$) fit (dotted black lines). We find that while the stellar masses determined in the test cases are consistent with the fits using the known redshifts, the true redshift was harder to constrain in the test cases.

extremely faint hosts in the absence of a subarcsecond localization (e.g., Eftekhari & Berger 2017).

In Figures 7 and 8, we show optical afterglow luminosities and projected physical offsets (in kiloparsecs) of the faint host short GRBs in comparison to those of the rest of the short GRB sample from Fong et al. (2022) and Nugent et al. (2022) at a common rest-frame time of $t_{RF} \sim 3$ hr. We determine luminosities at the common rest-frame time by: (i) fitting the observed afterglow data with a declining power-law model ($F_\nu \propto t^\alpha$; where α is typically a negative number) when there are multiple detections in a single optical filter (prioritizing r band) and (ii) fitting the observed afterglow data with a $F_\nu \propto t^{-1}$ power-law decline when there is only one detection (e.g., $\alpha = -1$). If a short GRB has no detected optical afterglow, we include only the deepest luminosity upper limit that was ±2.5 hr from the common rest-frame time. All optical afterglow data for the faint host short GRBs are from Levan et al. (2006), Berger (2007), Piranomonte et al. (2008), Perley et al. (2009), Butler et al. (2013), Littlejohns et al. (2013), Tanvir et al. (2013), Tunnicliffe et al. (2014), Knust et al. (2017), Jin et al. (2018), Rastinejad et al. (2021), and Laskar et al. (2022), and all other optical afterglow data are from Rastinejad et al. (2021) and references therein.

We show CDFs of optical afterglow luminosities for the 10 bursts from the faint host sample with detected optical afterglows (corrected to $t_{RF} \sim 3$ hr), along with the rest of the short GRB population (Figure 7). We find that the faint host short GRBs have a median and population 68% confidence interval of $\log(L_{opt}) \approx 43.27 \pm 0.81$ erg s^{-1} with the `Prospector-β` ($M_*–r_e$) redshifts[10] and a slightly higher $\log(L_{opt}) \approx 43.78 \pm 0.62$ erg s^{-1} from the `Prospector-β` redshifts. In either case, they are similar to the optical afterglow luminosities for the rest of the population, which has a median and 68% confidence interval of $\log(L_{opt}) \approx 43.65 \pm 0.78$ erg s^{-1}. To test if these differences are statistically significant, we perform an

Anderson–Darling (A-D) test between the distributions of detected short GRB optical afterglow luminosities. We find that $P_{AD} = 0.25$ when using the `Prospector-β` ($M_*–r_e$) relation redshifts, and $P_{AD} = 0.18$ when using the `Prospector-β` redshifts. The resulting probabilities of $P_{AD} > 0.05$ show that we cannot reject the null hypothesis that the afterglow luminosities are derived from the same underlying distribution. Thus, we find that the faint host short GRBs have statistically similar optical afterglows to the rest of the short GRB population.

However, we note that in this comparison, we are neglecting the majority of the short GRB population that only have upper limits on optical afterglow emission, and thus the gray distribution represents an upper limit. Therefore, it is possible that the optical afterglows of the faint host population are intrinsically brighter than those from more massive hosts.

We show the optical afterglow luminosities versus projected physical offsets in Figure 8 (inferred from both the `Prospector-β`– and `Prospector-β` ($M_*–r_e$)–determined redshifts). While their afterglows appear more similar to the short GRB population, their offsets are much smaller. To compare the offset distributions more rigorously, we plot the CDFs of projected physical and host-normalized offsets in Figure 9. We create CDFs for both the observed offsets and the observed offsets including their 1σ uncertainties, which are built from 5000 realizations on a Rice distribution (see Equation (2) in Blanchard & Berger 2016; Section 6.2 in Fong et al. 2022, for more details). We find for the `Prospector-β` redshifts, the observed projected physical offset median is $2.87^{+0.94}_{-2.1}$ kpc, and when including the uncertainties, the median changes to $2.7^{+1.45}_{-1.96}$ kpc. When using the `Prospector-β` ($M_*–r_e$) redshifts, we find similar results: the observed median lies at $2.24^{+0.74}_{-1.61}$ kpc, and with uncertainties, $2.01^{+1.13}_{-1.37}$ kpc. The rest of the short GRB sample resides at larger projected physical offsets: $9.6^{+21.6}_{-7.5}$ kpc (observed) and $12.1^{+23.0}_{-9.3}$ kpc (with uncertainties). We note that the median projected physical offset for the rest of the short GRB population is larger than

---

[10] Here and onward, we use the known spectroscopic redshifts for GRBs 090426A and 131004A in our calculations.
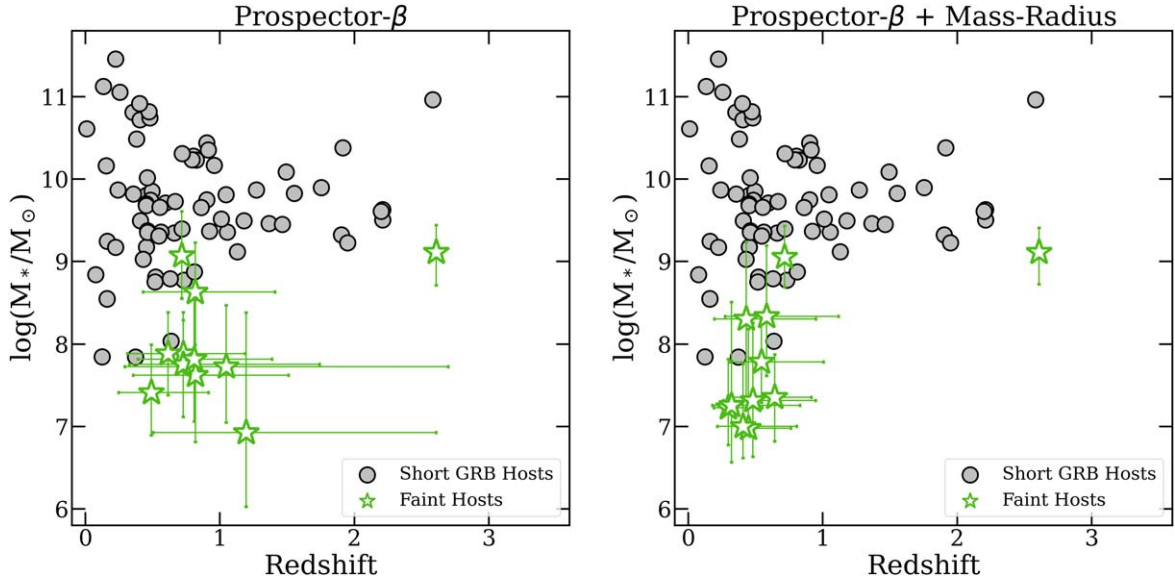
Figure 5. Left: the stellar masses ($\log(M_*/M_\odot)$) and redshifts of the faint host galaxy population (green stars) estimated from the Prospector-β fits, in comparison to the full short GRB host sample, with the same coloring as Figure 1. Right: the same figure, but with stellar masses and redshifts estimated from the Prospector-β (M_*-r_e) fit. We see in both cases this population trends toward lower stellar masses than the full host sample, with more moderate redshifts, in line with expectations from the full host sample.
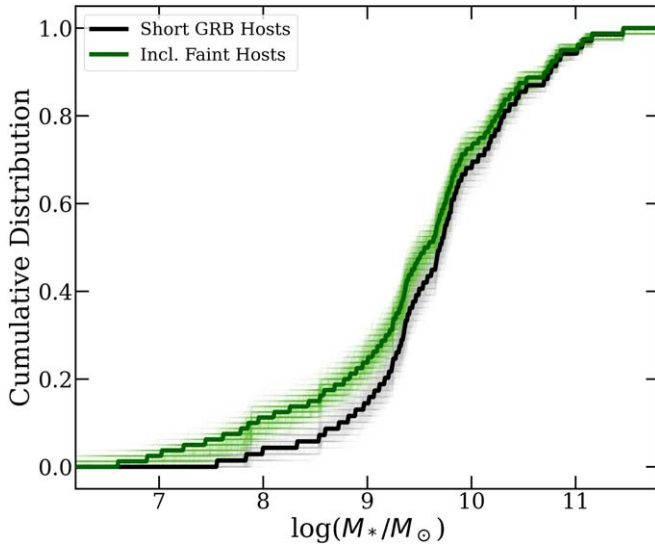
Figure 6. The cumulative distribution function (CDF) in stellar mass of the short GRB sample in Nugent et al. (2022; gray lines) and the effect of including the faint host short GRB sample (green lines). We only show the effect from the Prospector-β (M_*-r_e) fits as both stellar population modeling methods result in the same effect to the stellar mass distribution. The darker lines represent the median of the CDF and the lighter lines show 5000 realizations of the CDF. We find that while the stellar mass distribution stays similar to the results of Nugent et al. (2022), the tail of the CDF is extended toward lower masses.
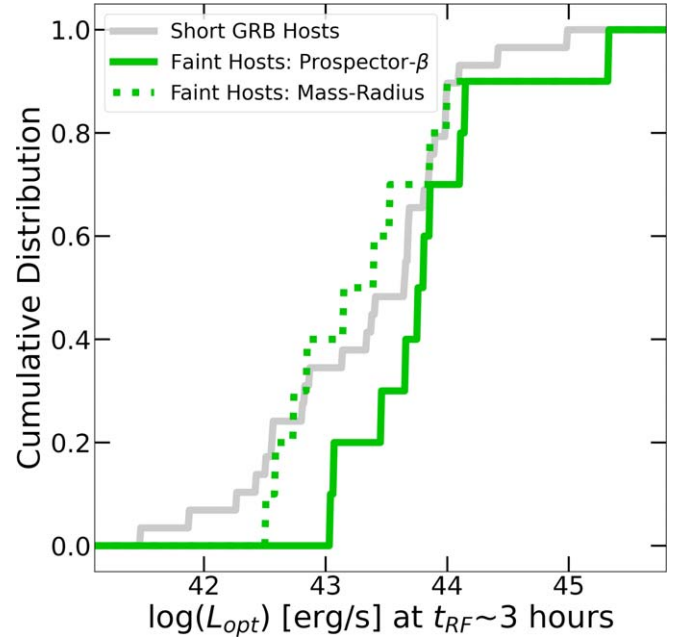

Figure 7. The CDFs of the detected optical afterglow luminosities from the faint host short GRBs (green) in comparison the rest of the short GRB population (gray). The straight line represents afterglow luminosities inferred from the Prospector-β redshifts, and the dotted line represents those inferred from the Prospector-β (M_*-r_e) redshifts. The gray line in this case can be treated as an upper limit on the distribution of short GRB optical afterglows, given that it neglects the $\sim$60% of short GRBs that only have upper limits. The short GRBs in the faint hosts have similar optical afterglow luminosities than the rest of the short GRBs from their inferred redshifts.

that reported in Fong et al. (2022) as we are no longer including the sample studied here in that population estimate. When we do include our sample, the median for all short GRB projected physical offsets is the same as that in Fong et al. (2022), $\approx$7.7 kpc. We compute P_{AD} between the distributions (with one test for each of the 5000 realizations on the CDF), and find that all tests result in $P_{AD} < 0.05$, demonstrating that they are statistically distinct.

We further compare the offsets for all short GRBs in a host with $M_* \leqslant 10^9\, M_\odot$ (a total of 21 hosts), which increases the the

median of the observed offsets of short GRBs in dwarfs to $2.56^{+6.13}_{-1.72}$ kpc ($2.93^{+6.14}_{-2.09}$ kpc with uncertainties) when using the Prospector-β (M_*-r_e) redshifts, and $2.95^{+6.23}_{-1.98}$ kpc ($3.31^{+5.72}_{-2.35}$ kpc with uncertainties) when using the Prospector-β redshifts. This is plotted as the purple distribution in Figure 9. A-D tests between this population and the full
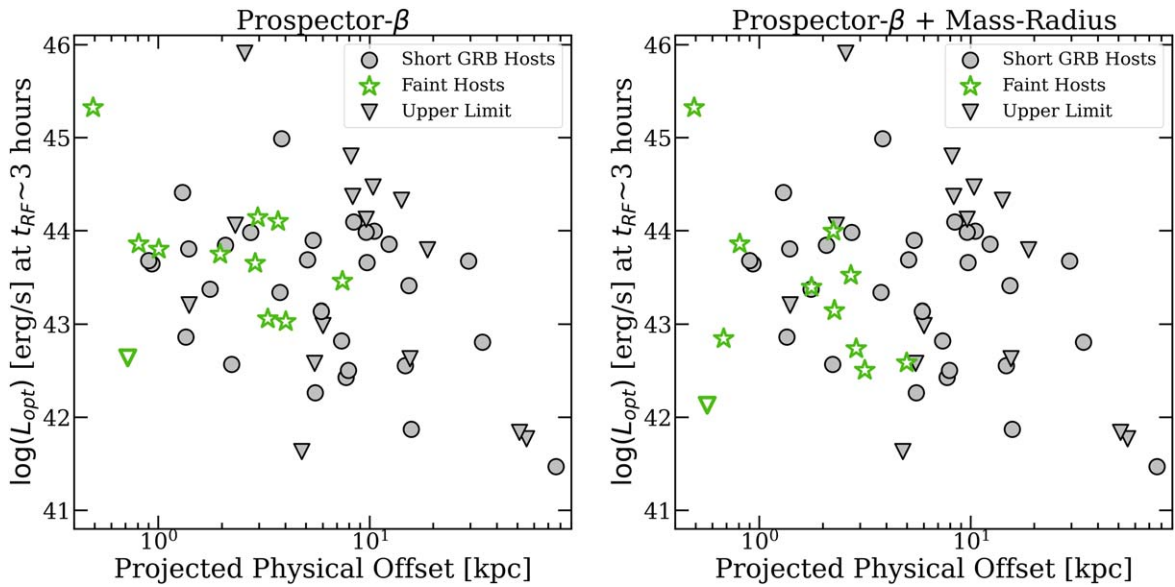
Figure 8. Left: the optical afterglow luminosities of the faint host short GRB sample (green stars) inferred from the `Prospector-β` redshifts in comparison the full short GRB sample (gray circles) vs. the observed physical projected offsets in kiloparsecs. Upper limits on luminosity are denoted with downward triangles. Right: the same as the left, but with the faint host short GRB optical afterglow luminosities determined from the `Prospector-β` (M_*–r_e) redshifts. We find that the faint host short GRBs have smaller physical offsets and similar afterglow luminosities in comparison to the rest of the short GRB sample. We also see an apparent trend of higher optical afterglow luminosities correlating to smaller offsets with this sample.

sample of short GRB offsets still results in $P_{AD} < 0.05$. This signifies that short GRBs identified in low-mass hosts have smaller offsets than those identified in higher-mass hosts.

When normalized by the sizes of the hosts, the same trend holds although the difference is less distinct: the faint host short GRBs have an observed median of $1.19^{+0.48}_{-0.92}r_e$ ($1.17^{+0.70}_{-0.91}r_e$ with uncertainties), and the rest of the short GRBs have an observed median of $2.0^{+2.87}_{-1.31}r_e$ ($2.21^{+2.78}_{-1.53}r_e$ with uncertainties). We find that 60% of the A-D tests result in $P_{AD} < 0.05$. This suggests that the faint host short GRB hosts indeed occur closer to their host centers than the rest of the short GRB population. Given that there are higher ISM densities toward the center of galaxies, this may also explain why the majority of these short GRBs have detectable optical afterglows. We discuss the implications for these results in the context of dwarf hosts in Section 6.

5.2. Assessing Contamination from Collapsar Events

With their low inferred stellar masses and smaller offsets, the faint host short GRB sample is reminiscent of the properties of long GRBs (Fruchter et al. 2006; Kelly et al. 2008; Kann et al. 2011; Blanchard & Berger 2016; Lyman et al. 2017; Audcent-Ross et al. 2020), which typically have gamma-ray durations $t_{90} \gtrsim 2$ s and are from the collapse of massive stars (e.g., MacFadyen & Woosley 1999). In particular, long GRBs are more likely to reside in dwarf and lower-mass galaxies than short GRBs (Svensson et al. 2010; Perley et al. 2013; Wang & Dai 2014; Vergani et al. 2015; Niino et al. 2017; Schulze et al. 2021; Taggart & Perley 2021; Nugent et al. 2022). Thus, a natural explanation is that the short GRBs from the faint host sample are actually collapsar events from massive stellar deaths. Here, we comment on this possibility. First, we find that the majority of the 11 GRBs with faint hosts have typical gamma-ray durations spanning $0.2 \leqslant t_{90} \leqslant 1.97$ s (Lien et al. 2016). Two GRBs in this sample (GRBs 080503 and 150424A)

are classified as short GRBs with extended emission, and both have $t_{90} \geqslant 81$ s.

Beyond durations, we can look at the classification criteria put forth by Bromberg et al. (2013), which is based on a broader range of gamma-ray properties. Using the probabilities in Appendix B of Fong et al. (2022), seven of the short GRBs in our sample have recorded f_{NC} values (GRBs 060313, 090305, 090426A, 091109B, 130912A, 131004A, and 211106A), where f_{NC} is the probability of not originating from a collapsar (e.g., a high probability indicates a merger origin). Of these, five have $f_{NC} \geqslant 0.69$, where three of which have very robust, "Gold" host associations. The two remaining events have lower values for f_{NC}: GRBs 090426A ($f_{NC} = 0.1$) and 131004A ($f_{NC} = 0.05$); these are also the two bursts with known redshift. Thus, any possible contamination from collapsar events is likely small and does not affect our overall results.

6. Discussion

6.1. Selection Effects

Before discussing implications, it is useful to explore the selection effects of this sample. As a population, the 11 short GRBs studied here generally have smaller galactocentric offsets (see Section 5.1) than the rest of the short GRB population. Because the probability of chance coincidence (P_{cc}) host association method relies on a combination of apparent magnitude and projected angular offset (Bloom et al. 2002), and all of the hosts in this sample are by default apparently faint, it is natural to expect that most of the short GRBs firmly associated with dwarf galaxies are at small angular offsets. Indeed, for a short GRB at the median angular offset of $\approx 1''.2$ (Fong et al. 2022) from a $r = 27$ mag host, $P_{cc} = 0.20$, making this a fairly insecure host association. In contrast, the angular offsets of this sample are all $\lesssim 0''.9$. Thus, the discovery of a population of short GRBs with dwarf host galaxies at small offsets does not preclude a missing population at larger offsets.
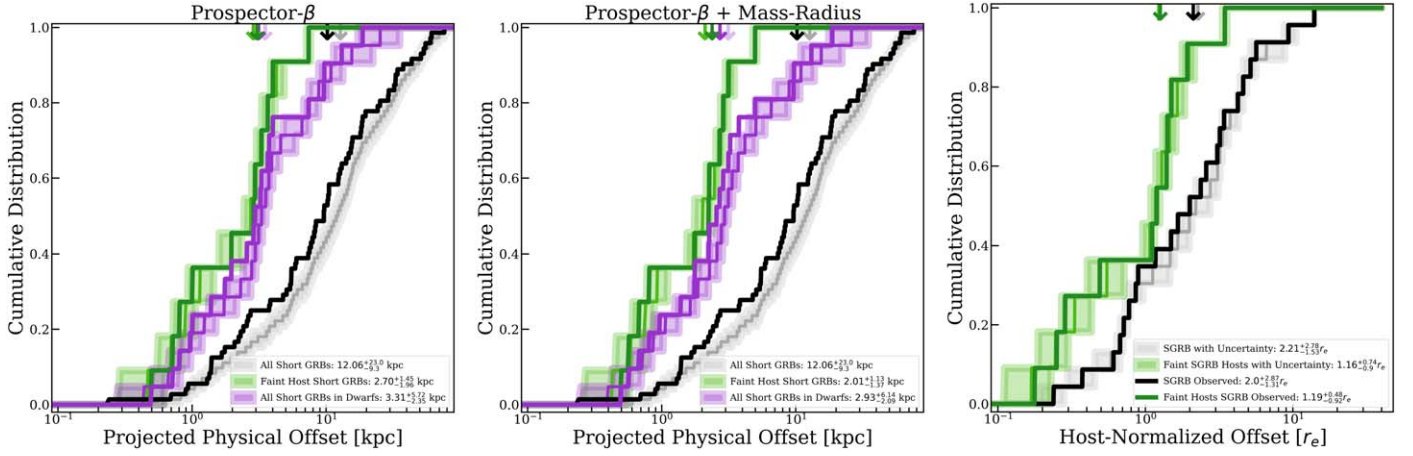
Figure 9. Left: the projected physical offset CDF for the faint host short GRBs (the observed CDF in dark green; with 1σ uncertainties, the CDF is in light green) inferred from the `Prospector-β` redshifts in comparison to that of the rest of the short GRB population (observed CDF in black; with 1σ uncertainties, the CDF is given in gray) and all short GRBs in dwarfs (observed CDF in purple; with uncertainties, the CDF is shown in light purple). The legend refers to the population median and 68% confidence interval. Middle: the same as the left, but with the faint host short GRB physical offsets inferred from the `Prospector-β` and mass–radius relation redshifts. Right: the host-normalized (galactocentric) offsets, which are independent of redshift, with the same colors as the previous plots. The arrows at the top of each plot represent the median of each of the distributions. We find that the faint host short GRBs are both occurring at smaller physical and host-normalized offsets than the rest of the short GRB population.

Indeed, one might expect that NS mergers in dwarf galaxies have larger offsets than in more massive hosts. Given the relatively shallow potential wells of dwarf galaxies, kicks at BNS formation may readily eject them from their hosts (Belczynski et al. 2006; Safarzadeh et al. 2019). In fact, our findings imply that we *are* missing a population of dwarf hosts in current short GRB studies.

We briefly explore the current population of Swift short GRBs to search for such a population. The 10 other short GRBs discovered known to have $M_* < 10^9 \, M_\odot$ dwarf hosts (Nugent et al. 2022) have higher projected physical offsets than the sample studied here, with a population median of 3.51 kpc, and range of 0.97–18.75 kpc (Fong et al. 2022). Notably, seven of these are "Gold" sample host associations, likely owing to the fact that these galaxies are apparently brighter than the sample studied here, and thus are easier to associate. Two of these short GRBs have offsets > 10 kpc and could be examples of NS mergers that were ejected from their dwarf hosts. In general, the larger observed offsets for the rest of the short GRB in dwarfs sample could simply be a consequence of the galaxies having slightly larger stellar mass (median $M_* \approx 10^{8.6} \, M_\odot$), and thus larger radii, than the sample studied here. Thus, the majority of these short GRBs could still be retained within their (slightly) larger hosts but lack high-resolution data to enable host-normalized radii measurements to test this.

We further note that Fong et al. (2022) accounted for six short GRBs that have inconclusive host associations (GRBs 061201, 110112A, 140516A, 150423A, 160927A, and 160410A), five of which have subarcsecond localizations with optical afterglows. If there are underlying hosts, they all have optical magnitudes similar to the sample studied here ($\gtrsim 26$ mag), and could represent a population of dwarf hosts; however unless the angular offsets are small, it would be difficult to associate these with a faint host firmly. One short GRB with an inconclusive host furthermore has a spectroscopic redshift from its afterglow: GRB 160410A at $z = 1.717$ (Agüí Fernández et al. 2023), with no host detected to $r > 27.2$ mag. The very low inferred luminosity of $L \lesssim 10^9 \, L_\odot$ almost certainly puts any unseen host of GRB 160410A in the

dwarf-galaxy regime. Another option is it was ejected from a more nearby, massive galaxy, but no obvious candidate exists (Fong et al. 2022; Agüí Fernández et al. 2023). Furthermore, if the five other short GRBs are not observed to have coincident underlying galaxies, it implies that they were kicked out from a galaxy at a larger angular offset. Thus, studying the larger-scale environments surrounding these GRBs and determining if there are any dwarf galaxies in the field may better constrain the fraction of highly offset NS mergers in dwarf hosts.

6.2. Delay Times and Systemic Velocities

Finding a population of small-offset short GRBs, assumed to be from NS mergers, in dwarf galaxies has unique implications for their post-SN systemic velocities and delay times. As we mentioned in Section 6.1, we expect that dwarf galaxies in general will have very small escape velocities. Therefore, any NS merger that has been retained within a centralized location likely had a small SN natal kick (Bloom et al. 1999; Perna & Belczynski 2002; Zemp et al. 2009; Kelley et al. 2010; Behroozi et al. 2014; Wiggins et al. 2018; Andrews & Zezas 2019; Zevin et al. 2020). We note, however, that this is not necessarily a straightforward comparison, as the post-SN systemic velocity (relative to the local standard of rest at the location of the BNS-forming SN) depends on the interplay of SN natal kick, mass lost in the SN, and pre-SN orbital separation. Moreover, the distance traveled by the post-SN NS system, and whether it escapes from the galactic potential, depends on the direction of the post-SN systemic velocity relative to the pre-SN galactic motion; radial post-SN trajectories (i.e., perpendicular to the pre-SN motion) are not necessarily the optimal means of making a system migrate far distances from a host galaxy (Mandel 2016). Lastly, for systems with long delay times, galactic evolution plays an important role in the kinematic evolution of kicked systems; see e.g., Abbott et al. (2017b) and Zevin et al. (2020) for a deeper discussion of these effects.

Nevertheless, we perform a simple demonstration to showcase the interplay between systemic velocity and inspiral time of the short GRB dwarf host sample studied here. If we assume

that their NS merger progenitors have radial post-SN systemic velocities that exceed their host escape velocities *and* that they traveled from their hosts' effective radii toward their observed physical offset, we can derive a maximum inspiral time. To estimate the host escape velocities, we use a Hernquist density profile (Hernquist [1990]) at the median stellar mass and the median physical size derived for each host (Table [2]). We calculate a median escape velocity of $v_{esc} \approx 14$ km s^{-1} and population range of $5.5 \leqslant v_{esc} \leqslant 80$ km s^{-1}, with the range based on variations of the Hernquist potential scale parameter.[11] We note that systemic velocities inferred for Galactic and extragalactic NS systems tend to be higher than these escape velocities. For example, Galactic NS systems have been constrained to systemic velocities ranging over 25–240 km s^{-1} (Fryer & Kalogera [1997]; Wex et al. [2000]; Wong et al. [2010]; Tauris et al. [2017]). For the short GRB population, Fong & Berger ([2013]) place systemic velocity constraints ranging $20 < v < 140$ km s^{-1}, while Zevin et al. ([2020]) find two highly offset (>34 kpc) GRBs (GRBs 070809 and 090515) in old, quiescent, and $>10^{10.8}$ $M_{\odot}$ hosts, which likely have systemic velocities of $v > 200$ km s^{-1}.

Using the median escape velocities of our short GRB hosts (14 km s^{-1}) as an estimate for the smallest velocity to escape their host (corresponding to the longest inspiral time for escaping systems to reach a particular distance), and the median of their distance traveled from the hosts' effective radii (≈ 1.1 kpc) as their radial distance, we find that the maximum inspiral is ≈ 77 Myr. We note that if the systemic velocities were significantly higher than their host escape velocities (e.g., more similar to the observed systemic velocities of NS systems), these systems still could have merged at small offsets due to extremely short inspiral times. Without a direct probe of the inspiral time or systemic velocity, we cannot disentangle whether these systems had systemic velocities significantly lower than their host escape velocities, and thus merged at long timescales, or if they had large systemic velocities and short timescales. Constraining the SFHs of these hosts with high-quality spectroscopic observations from JWST will lend more conclusive inferences on the inspiral times and systemic velocities of these systems.

6.3. Implications for GW Follow-up

Given large localization regions of mergers with current GW detectors (>1000 deg^2 for NS mergers in the LIGO/Virgo fourth observing run; Abbott et al. [2018], [2020]; Petrov et al. [2022]), there is a need to constrain events to only their possible host galaxies to reduce the area in which to search for electromagnetic counterparts. These methods have typically relied on ranking galaxies in a field by their *B*-band luminosity, which traces star formation, or *K*-band luminosity, which traces stellar mass (White et al. [2011]; Blanchard et al. [2017]; Palmese et al. [2017]; Dálya et al. [2018]; Ebrová et al. [2020]; Kilpatrick et al. [2022]). For NS mergers, galaxies with larger stellar masses and less star formation are generally ranked higher as possible host galaxies. Indeed, this method proved worthwhile in the case of GW 170817, where its host NGC 4993 was ranked high as a possible host for the event (Arcavi et al. [2017]; Coulter et al. [2017]; Ducoin et al. [2020]). However, given that short GRBs trace both star formation and stellar mass (Nugent et al. [2022]), we do

not expect their hosts to always be the brightest and most massive in the field.

The addition of more dwarf hosts in this population further justifies that ranked-based methods on *B*- or *K*-band luminosities will not always be successful, as short GRBs can occur in a wider range of environments than previously thought. Assuming that we are missing a number of dwarf hosts due to larger short GRB offsets and fainter afterglow luminosities (see Section [6.1]), we also may infer that the stellar mass distribution shown in Figure [6] shifts even further toward lower stellar mass solutions. Taken together with the fact that dwarf galaxies are the most common galaxies across all redshifts (Bullock & Boylan-Kolchin [2017]), it is quite possible that at least a fraction of NS mergers within the LIGO/Virgo GW volume will be located in dwarf hosts. Thus, galaxy-targeted searches for counterparts of GW events should be aware of this diversity when utilizing rank-based methods.

6.4. r-Process in Dwarf Galaxies

With this work, we have shown strong observational support that at least some NS mergers can occur and be retained within dwarf galaxies. These results challenge the notion that NS mergers are expected to experience strong natal kicks and long delay times, and thus likely would become unbound from dwarf hosts (Beniamini et al. [2016]; Bramante & Linden [2016]; Tauris et al. [2017]). While it is not currently clear whether the small offsets we observe for this short GRB sample are due to small natal kicks, short inspiral times, or both (see Section [6.2]), we can infer that one of these factors is occurring to explain our observations. Future JWST observations of the host galaxies studied here could be used to determine their SFHs, which would then enable inferences on the delay times and systemic velocities for these short GRB progenitors. In either case, our findings lend confidence to the possibility for NS mergers to enrich dwarf galaxies with *r*-process elements, and offer a natural explanation for those observed in Local Group dwarf galaxies (e.g., Ji et al. [2016a]; Duggan et al. [2018]; Matsuno et al. [2021]; Molero et al. [2021]; Reggiani et al. [2021]; Naidu et al. [2022]; Limberg et al. [2023]). Our study adds to the body of work on cosmological short GRB hosts and Local Group dwarf galaxies, from which we can infer that NS mergers are an observed source of *r*-process element production in galaxies of all masses and at all redshifts.

7. Conclusions

In this paper, we have used novel stellar population modeling techniques to infer the redshifts and stellar masses of 11 of the faintest short GRB host galaxies, with optical and near-infrared magnitudes > 25.5. This sample was selected based on their faintness in comparison to the rest of the observed short GRB host population (Fong et al. [2022]; O'Connor et al. [2022]), their lack of previous redshift and/or stellar mass estimates, and their effective radii measurements from available HST data. We list our main conclusions below.

1. We develop new stellar population modeling techniques that build upon the current Prospector-β infrastructure (Wang et al. [2023a]). In particular, we implement the van der Wel et al. ([2014]) mass–radius relation to weight more strongly the probabilities of Prospector-β stellar mass and redshift solutions that result in effective radii compatible

---

[11] Here, we neglect the contribution of the dark matter halo in this simple estimate.

to the observed measurements. We generally find that the stellar mass estimates from this method are robust.

2. For the 11 faint hosts studied here, assuming they are drawn from the field galaxy population, we derive a median and 68% population confidence interval of $\log(M_*/M_\odot) = 7.79^{+1.22}_{-0.84}$ and redshift $z = 0.54^{+0.42}_{-0.29}$ when implementing the M_*–r_e relation. We find stellar mass to be a fairly robust parameter, and conclude that this is a population of dwarf-galaxy hosts.

3. In comparison to the rest of the short GRB host population, these hosts have redshifts similar to the observed median ($z \approx 0.64$), but are within the bottom $\approx 14\%$ of stellar mass estimates. Combined with 10 short GRBs with brighter apparent magnitudes but low stellar masses of $M_* \lesssim 10^9 \ M_\odot$, we derive a lower limit on the fraction of Swift short GRBs occurring in dwarf galaxies of $\gtrsim 13.5\%$.

4. We find that the faint host population has similar optical afterglow luminosities to the rest of the population. However, this comparison neglects the fact that the majority of short GRBs lack optical afterglow detections. Thus, when incorporating these limits, it is possible that the faint host population has more luminous afterglows.

5. Short GRBs in faint hosts exhibit smaller projected physical and host-normalized offsets than the rest of the short GRB population. We thus infer that the majority of the short GRBs in the faint hosts were retained within their host galaxies and could represent a population of low kick velocity progenitors or those with very short delay times. This is commensurate with their (possibly) more luminous afterglows.

6. Given that many Galactic BNS systems have velocities $\gtrsim 100 \ \mathrm{km \ s^{-1}}$, and escape velocities in dwarf galaxies are likely much lower, its possible many NS systems in dwarfs have been kicked out. Consequently, such systems exist at larger offsets, making robust host association extremely challenging. With this logic, it is likely that a fraction of dwarf hosts are missing from the current short GRB host sample.

Overall, our analysis provides the first strong observational support of a population of short GRBs in dwarf galaxies. As there is broad consensus that most short GRBs originate from NS mergers, this indicates that NS mergers are a viable source of r-process enrichment in these low-mass environments. Moreover, we demonstrate that at least a fraction of NS mergers can be retained in these environments. Indeed, our sample of faint host short GRBs may be representative analogs to the r-process event in Reticulum II and other dwarf galaxies. Our work furthermore paves the way for stellar mass and redshift estimates of faint galaxies with very sparse photometric coverage, given our novel implementation of the van der Wel et al. (2014) mass–radius relation into Prospector-β.

The next natural step is to obtain spectra of the sample of low-mass hosts studied here to determine their true redshifts, metallicities, and SFHs. In particular, host galaxy SFHs can constrain NS merger delay times, from which we can infer the degree of r-process enrichment by NS mergers in very young, low-metallicity environments. Then, we can begin to answer what fraction of r-process elements in the Universe are derived from NS merger channels, as opposed to other proposed mechanisms. JWST will be instrumental in the pursuit of these answers, as it has already proven to observe high-quality spectra for even the faintest, highest-redshift galaxies. We finally note that continued observations, follow-up, and host galaxy associations of short GRBs are needed to expand upon this faint host population and infer the fraction of dwarf hosts that are missing in current host studies.

Appendix
Mass–Radius Relation Implementation

To correlate the van der Wel et al. (2014) mass–radius relation with our Prospector-derived results and determine which solutions are reasonable given the size of each host, we include a likelihood function of the physical r_e of a host derived
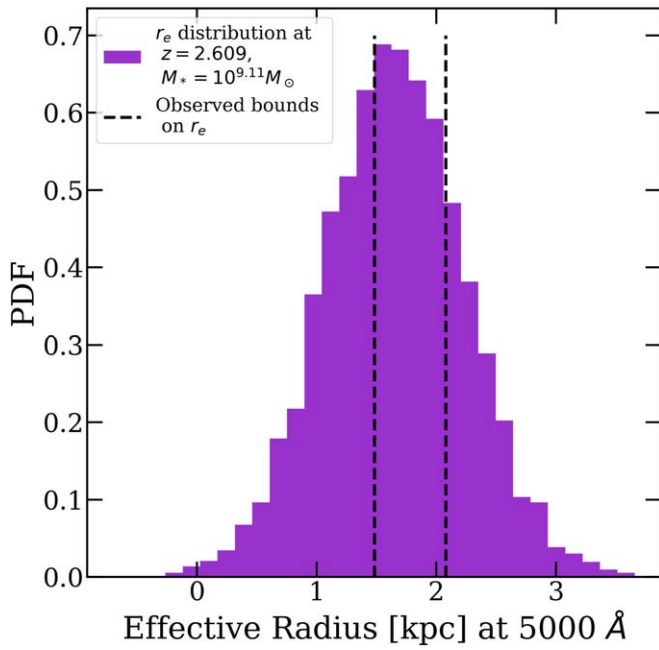
Figure A1. A representation of the distribution of effective radii (purple histogram) from the van der Wel et al. (2014) mass–radius (Equation (A1)) relation at $z = 2.609$, and $M_* = 10^{9.11} M_\odot$, which are the known redshift and median stellar mass of GRB 090426A's host. We further show the bounds on the corrected effective radii at 5000 Å (Equation (A2)), from the observed angular effective radius of GRB 090426A's host at this redshift and stellar mass (black dashed lines).

from `Prospector`-sampled mass and redshift in the nested-sampling fitting routine. The current nested-sampling routine in `Prospector` derives the likelihood of a model SED inferred from a sample of prior distributions, given its fit to the observed SED. Using similar logic, we include the angular r_e in arcseconds and the central wavelength of the filter where that measurement was taken as observed data for the host, along with its photometry. At a `Prospector`-sampled M_F (which is converted to M_* within the fitting) and z, we determine the mean physical r_e and 1σ confidence interval, using:

$$\frac{r_e}{\text{kpc}} = A \times \left(\frac{M_*}{5 \times 10^{10} M_\odot}\right)^\alpha. \qquad (A1)$$

Here, r_e represents the physical r_e at rest-frame 5000 Å, and the values for A, α, and the Gaussian 1σ scatter ($\sigma \log r_e$) on the mass–radius relationship are given in Table 1 in van der Wel et al. (2014) at various redshifts over $0 < z < 3$ for late-type and early-type galaxies. We assume that the galaxies are all late-type, which is a reasonable assumption for our sample given that the hosts are likely dwarfs at moderate redshift or high redshift; in both cases, early-type galaxies are rare. Then, we convert the observed angular r_e to a physical r_e at z, and correct it to a physical r_e at rest-frame 5000 Å using Equation (1) in van der Wel et al. (2014):

$$\frac{\Delta \log r_e}{\Delta \log \lambda} = -0.35 + 0.12z - 0.25 \log \frac{M_*}{10^{10} M_\odot}. \qquad (A2)$$

Using Figure 4 in van der Wel et al. (2014), we also find the 1σ scatter on this correction given the sampled stellar mass, then sample 10,000 r_e from a Gaussian distribution using the mean r_e from Equation (A2) and the 1σ scatter. We finally determine

the likelihood for each of these 10,000 observed physical r_e from a Gaussian distribution given the mean and 1σ using Equation (A1) with the sampled M_* and z, and determine the average likelihood. We show an example of the distribution of effective radii for sampled M_* and z, and the bounds determined from the mean and 1σ observed r_e in Figure A1. The final log-likelihood of the sampled point then becomes the log-likelihood of the model SED added to the log-likelihood determined from the mass–radius relation.

ORCID iDs

Anya E. Nugent ⓘ https://orcid.org/0000-0002-2028-9329
Wen-fai Fong ⓘ https://orcid.org/0000-0002-7374-935X
Cristian Castrejon ⓘ https://orcid.org/0009-0005-4757-8285
Joel Leja ⓘ https://orcid.org/0000-0001-6755-1315
Michael Zevin ⓘ https://orcid.org/0000-0002-0147-0835
Alexander P. Ji ⓘ https://orcid.org/0000-0002-4863-8842

References

Abbott, B. P., Abbott, R., Abbott, T. D., et al. 2017a, ApJL, 848, L13
Abbott, B. P., Abbott, R., Abbott, T. D., et al. 2017b, ApJL, 850, L40
Abbott, B. P., Abbott, R., Abbott, T. D., et al. 2018, LRR, 21, 3
Abbott, B. P., Abbott, R., Abbott, T. D., et al. 2020, LRR, 23, 3
Agüí Fernández, J. F., Thöne, C. C., Kann, D. A., et al. 2023, MNRAS, 520, 613
Akins, H. B., Casey, C. M., Allen, N., et al. 2023, ApJ, 956, 61
Anand, N., Shahid, M., & Resmi, L. 2018, MNRAS, 481, 4332
Andrews, J. J., & Mandel, I. 2019, ApJL, 880, L8
Andrews, J. J., & Zezas, A. 2019, MNRAS, 486, 3213
Arcavi, I., McCully, C., Hosseinzadeh, G., et al. 2017, ApJL, 848, L33
Argast, D., Samland, M., Thielemann, F. K., & Qian, Y. Z. 2004, A&A, 416, 997
Audcent-Ross, F. M., Meurer, G. R., Audcent, J. R., et al. 2020, MNRAS, 492, 848
Behroozi, P. S., Ramirez-Ruiz, E., & Fryer, C. L. 2014, ApJ, 792, 123
Belczynski, K., Kalogera, V., & Bulik, T. 2002, ApJ, 572, 407
Belczynski, K., Perna, R., Bulik, T., et al. 2006, ApJ, 648, 1110
Beniamini, P., Hotokezaka, K., & Piran, T. 2016, ApJ, 832, 149
Beniamini, P., & Piran, T. 2019, MNRAS, 487, 4847
Bennett, C. L., Larson, D., Weiland, J. L., & Hinshaw, G. 2014, ApJ, 794, 135
Berger, E. 2007, ApJ, 670, 1254
Berger, E. 2010, ApJ, 722, 1946
Berger, E. 2014, ARA&A, 52, 43
Berger, E., Fox, D. B., Price, P. A., et al. 2007, ApJ, 664, 1000
Blanchard, P. K., & Berger, E. 2016, ApJ, 817, 144
Blanchard, P. K., Berger, E., Fong, W., et al. 2017, ApJL, 848, L22
Blanchard, P. K., Villar, V. A., Chornock, R., et al. 2023, arXiv:2308.14197
Bland-Hawthorn, J., Sutherland, R., & Webster, D. 2015, ApJ, 807, 154
Bloom, J. S., Kulkarni, S. R., & Djorgovski, S. G. 2002, AJ, 123, 1111
Bloom, J. S., Sigurdsson, S., & Pols, O. R. 1999, MNRAS, 305, 763
Bramante, J., & Linden, T. 2016, ApJ, 826, 57
Brammer, G. B., van Dokkum, P. G., Franx, M., et al. 2012, ApJS, 200, 13
Brauer, K., Ji, A. P., Drout, M. R., & Frebel, A. 2021, ApJ, 915, 81
Bromberg, O., Nakar, E., Piran, T., & Sari, R. 2013, ApJ, 764, 179
Bullock, J. S., & Boylan-Kolchin, M. 2017, ARA&A, 55, 343
Butler, N., Watson, A. M., Kutyrev, A., et al. 2013, GCN, 15226, 1
Calzetti, D., Armus, L., Bohlin, R. C., et al. 2000, ApJ, 533, 682
Cardelli, J. A., Clayton, G. C., & Mathis, J. S. 1989, ApJ, 345, 245
Chornock, R., Berger, E., Kasen, D., et al. 2017, ApJL, 848, L19
Church, R. P., Levan, A. J., Davies, M. B., & Tanvir, N. 2011, MNRAS, 413, 2004
Conroy, C., & Gunn, J. E. 2010, ApJ, 712, 833
Conroy, C., Gunn, J. E., & White, M. 2009, ApJ, 699, 486
Côté, B., Fryer, C. L., Belczynski, K., et al. 2018, ApJ, 855, 99
Coulter, D. A., Foley, R. J., Kilpatrick, C. D., et al. 2017, Sci, 358, 1556
Cowan, J. J., Sneden, C., Lawler, J. E., et al. 2021, RvMP, 93, 015002
Dálya, G., Galgóczi, G., Dobos, L., et al. 2018, MNRAS, 479, 2374
D'Avanzo, P., Malesani, D., Covino, S., et al. 2009, A&A, 498, 711
De Pasquale, M. 2019, Galax, 7, 30
Dey, B., Andrews, B. H., Newman, J. A., et al. 2022, MNRAS, 515, 5285

Dominik, M., Belczynski, K., Fryer, C., et al. 2012, ApJ, 759, 52
Ducoin, J. G., Corre, D., Leroy, N., & Le Floch, E. 2020, MNRAS, 492, 4768
Duggan, G. E., Kirby, E. N., Andrievsky, S. M., & Korotin, S. A. 2018, ApJ, 869, 50
Ebrová, I., Bílek, M., Yıldız, M. K., & Eliášek, J. 2020, A&A, 634, A73
Eftekhari, T., & Berger, E. 2017, ApJ, 849, 162
Eichler, D., Livio, M., Piran, T., & Schramm, D. N. 1989, Natur, 340, 126
Falcón-Barroso, J., Sánchez-Blázquez, P., Vazdekis, A., et al. 2011, A&A, 532, A95
Ferro, M., Brivio, R., D'Avanzo, P., et al. 2023, A&A, 678, A142
Fong, W., & Berger, E. 2013, ApJ, 776, 18
Fong, W., Berger, E., Chornock, R., et al. 2013, ApJ, 769, 56
Fong, W., Berger, E., & Fox, D. B. 2010, ApJ, 708, 9
Fong, W., Berger, E., Margutti, R., & Zauderer, B. A. 2015, ApJ, 815, 102
Fong, W.-f., Nugent, A. E., Dong, Y., et al. 2022, ApJ, 940, 56
Fox, D. B., Frail, D. A., Price, P. A., et al. 2005, Natur, 437, 845
Fruchter, A. S., Levan, A. J., Strolger, L., et al. 2006, Natur, 441, 463
Fryer, C., & Kalogera, V. 1997, ApJ, 489, 244
Gallazzi, A., Charlot, S., Brinchmann, J., White, S. D. M., & Tremonti, C. A. 2005, MNRAS, 362, 41
Gehrels, N., Chincarini, G., Giommi, P., et al. 2004, ApJ, 611, 1005
Goldstein, A., Veres, P., Burns, E., et al. 2017, ApJL, 848, L14
Granot, J., & Sari, R. 2002, ApJ, 568, 820
Hao, J.-M., & Yuan, Y.-F. 2013, A&A, 558, A22
Häussler, B., McIntosh, D. H., Barden, M., et al. 2007, ApJS, 172, 615
Hernquist, L. 1990, ApJ, 356, 359
Hinshaw, G., Larson, D., Komatsu, E., et al. 2013, ApJS, 208, 19
Hotokezaka, K., Beniamini, P., & Piran, T. 2018, IJMPD, 27, 1842005
Jeon, M., Besla, G., & Bromm, V. 2021, MNRAS, 506, 1850
Jeong, S., & Lee, C.-H. 2010, JKPS, 56, 1619
Ji, A. P., Frebel, A., & Bromm, V. 2015, MNRAS, 454, 659
Ji, A. P., Frebel, A., Chiti, A., & Simon, J. D. 2016a, Natur, 531, 610
Ji, A. P., Frebel, A., Simon, J. D., & Chiti, A. 2016b, ApJ, 830, 93
Ji, A. P., Simon, J. D., Roederer, I. U., et al. 2023, AJ, 165, 100
Jin, Z.-P., Li, X., Wang, H., et al. 2018, ApJ, 857, 128
Johnson, B. D., Leja, J., Conroy, C., & Speagle, J. S. 2021, ApJS, 254, 22
Kann, D. A., Klose, S., Zhang, B., et al. 2011, ApJ, 734, 96
Kasen, D., Metzger, B., Barnes, J., Quataert, E., & Ramirez-Ruiz, E. 2017, Natur, 551, 80
Kelley, L. Z., Ramirez-Ruiz, E., Zemp, M., Diemand, J., & Mandel, I. 2010, ApJL, 725, L91
Kelly, P. L., Kirshner, R. P., & Pahre, M. 2008, ApJ, 687, 1201
Kilpatrick, C. D., Fong, W.-f., Blanchard, P. K., et al. 2022, ApJ, 926, 49
Knust, F., Greiner, J., van Eerten, H. J., et al. 2017, A&A, 607, A84
Koekemoer, A. M., Faber, S. M., Ferguson, H. C., et al. 2011, ApJS, 197, 36
Kriek, M., & Conroy, C. 2013, ApJL, 775, L16
Kriek, M., van Dokkum, P. G., Labbé, I., et al. 2009, ApJ, 700, 221
Labbé, I., van Dokkum, P., Nelson, E., et al. 2023, Natur, 616, 266
Laskar, T., Escorial, A. R., Schroeder, G., et al. 2022, ApJL, 935, L11
Lee, J. C., Gil de Paz, A., Kennicutt, C., Robert, J., et al. 2011, ApJS, 192, 6
Leibler, C. N., & Berger, E. 2010, ApJ, 725, 1202
Leja, J., Johnson, B. D., Conroy, C., et al. 2019, ApJ, 877, 140
Leja, J., Johnson, B. D., Conroy, C., Dokkum, P. G. v., & Byler, N. 2017, ApJ, 837, 170
Leja, J., Speagle, J. S., Johnson, B. D., et al. 2020, ApJ, 893, 111
Levan, A. J., Lyman, J. D., Tanvir, N. R., et al. 2017, ApJL, 848, L28
Levan, A. J., Tanvir, N. R., Fruchter, A. S., et al. 2006, ApJL, 648, L9
Lien, A., Sakamoto, T., Barthelmy, S. D., et al. 2016, ApJ, 829, 7
Limberg, G., Ji, A. P., Naidu, R. P., et al. 2023, arXiv:2308.13702
Littlejohns, O., Butler, N., Watson, A. M., et al. 2013, GCN, 15312, 1
Lyman, J. D., Levan, A. J., Tanvir, N. R., et al. 2017, MNRAS, 467, 1795
MacFadyen, A. I., & Woosley, S. E. 1999, ApJ, 524, 262
Mandel, I. 2016, MNRAS, 456, 578
Matsuno, T., Hirai, Y., Tarumi, Y., et al. 2021, A&A, 650, A110
McCully, C., Hiramatsu, D., Howell, D. A., et al. 2017, ApJL, 848, L32
McWilliam, A., Preston, G. W., Sneden, C., & Searle, L. 1995, AJ, 109, 2757
Molero, M., Romano, D., Reichert, M., et al. 2021, MNRAS, 505, 2913
Naidu, R. P., Ji, A. P., Conroy, C., et al. 2022, ApJL, 926, L36
Nakar, E., Gal-Yam, A., & Fox, D. B. 2006, ApJ, 650, 281
Nedkova, K. V., Häußler, B., Marchesini, D., et al. 2021, MNRAS, 506, 928
Niino, Y., Aoki, K., Hashimoto, T., et al. 2017, PASJ, 69, 27
Nugent, A. E., Fong, W.-F., Dong, Y., et al. 2022, ApJ, 940, 57
O'Connor, B., Troja, E., Dichiara, S., et al. 2022, MNRAS, 515, 4890
Ojima, T., Ishimaru, Y., Wanajo, S., Prantzos, N., & François, P. 2018, ApJ, 865, 87
Palmese, A., Hartley, W., Tarsitano, F., et al. 2017, ApJL, 849, L34
Paterson, K., Fong, W., Nugent, A., et al. 2020, ApJL, 898, L32
Paxton, B., Schwab, J., Bauer, E. B., et al. 2018, ApJS, 234, 34
Perets, H. B., & Beniamini, P. 2021, MNRAS, 503, 5997
Perley, D. A., Levan, A. J., Tanvir, N. R., et al. 2013, ApJ, 778, 128
Perley, D. A., Metzger, B. D., Granot, J., et al. 2009, ApJ, 696, 1871
Perna, R., & Belczynski, K. 2002, ApJ, 570, 252
Petrov, P., Singer, L. P., Coughlin, M. W., et al. 2022, ApJ, 924, 54
Pian, E., D'Avanzo, P., Benetti, S., et al. 2017, Natur, 551, 67
Piranomonte, S., D'Avanzo, P., Covino, S., et al. 2008, A&A, 491, 183
Qian, Y. Z. 2000, ApJL, 534, L67
Rastinejad, J. C., Fong, W., Kilpatrick, C. D., et al. 2021, ApJ, 916, 89
Reggiani, H., Schlaufman, K. C., Casey, A. R., Simon, J. D., & Ji, A. P. 2021, AJ, 162, 229
Safarzadeh, M., Ramirez-Ruiz, E., Andrews, J. J., et al. 2019, ApJ, 872, 105
Safarzadeh, M., & Scannapieco, E. 2017, MNRAS, 471, 2088
Savchenko, V., Ferrigno, C., Kuulkers, E., et al. 2017, ApJL, 848, L15
Schlafly, E. F., & Finkbeiner, D. P. 2011, ApJ, 737, 103
Schulze, S., Yaron, O., Sollerman, J., et al. 2021, ApJS, 255, 29
Selsing, J., Krühler, T., Malesani, D., et al. 2018, A&A, 616, A48
Shappee, B. J., Simon, J. D., Drout, M. R., et al. 2017, Sci, 358, 1574
Shetrone, M. D., Côté, P., & Sargent, W. L. W. 2001, ApJ, 548, 592
Siegel, D. M., Barnes, J., & Metzger, B. D. 2019, Natur, 569, 241
Skúladóttir, Á., Hansen, C. J., Salvadori, S., & Choplin, A. 2019, A&A, 631, A171
Speagle, J. S. 2020, MNRAS, 493, 3132
Svensson, K. M., Levan, A. J., Tanvir, N. R., Fruchter, A. S., & Strolger, L. G. 2010, MNRAS, 405, 57
Taggart, K., & Perley, D. A. 2021, MNRAS, 503, 3931
Tanvir, N. R., Levan, A. J., González-Fernández, C., et al. 2017, ApJL, 848, L27
Tanvir, N. R., Wiersema, K., & Levan, A. J. 2013, GCN, 15224, 1
Tarumi, Y., Yoshida, N., & Inoue, S. 2020, MNRAS, 494, 120
Tauris, T. M., Kramer, M., Freire, P. C. C., et al. 2017, ApJ, 846, 170
Tsujimoto, T., Ishigaki, M. N., Shigeyama, T., & Aoki, W. 2015, PASJ, 67, L3
Tunnicliffe, R. L., Levan, A. J., Tanvir, N. R., et al. 2014, MNRAS, 437, 1495
van der Wel, A., Bell, E. F., Häussler, B., et al. 2012, ApJS, 203, 24
van der Wel, A., Franx, M., van Dokkum, P. G., et al. 2014, ApJ, 788, 28
Venn, K. A., Shetrone, M. D., Irwin, M. J., et al. 2012, ApJ, 751, 102
Vergani, S. D., Salvaterra, R., Japelj, J., et al. 2015, A&A, 581, A102
Vigna-Gómez, A., Neijssel, C. J., Stevenson, S., et al. 2018, MNRAS, 481, 4009
Villasenor, J. S., Lamb, D. Q., Ricker, G. R., et al. 2005, Natur, 437, 855
Wanderman, D., & Piran, T. 2015, MNRAS, 448, 3026
Wang, B., Leja, J., Bezanson, R., et al. 2023a, ApJL, 944, L58
Wang, B., Leja, J., Labbé, I., et al. 2023b, ApJS, 270, 12
Wang, F. Y., & Dai, Z. G. 2014, ApJS, 213, 15
Wehmeyer, B., Pignatari, M., & Thielemann, F. K. 2015, MNRAS, 452, 1970
Wex, N., Kalogera, V., & Kramer, M. 2000, ApJ, 528, 401
White, D. J., Daw, E. J., & Dhillon, V. S. 2011, CQGra, 28, 085016
Wiggins, B. K., Fryer, C. L., Smidt, J. M., et al. 2018, ApJ, 865, 27
Williams, C. C., Curtis-Lake, E., Hainline, K. N., et al. 2018, ApJS, 236, 33
Wong, T.-W., Willems, B., & Kalogera, V. 2010, ApJ, 721, 1689
Zemp, M., Ramirez-Ruiz, E., & Diemand, J. 2009, ApJL, 705, L186
Zevin, M., Kelley, L. Z., Nugent, A., et al. 2020, ApJ, 904, 190
Zevin, M., Nugent, A. E., Adhikari, S., et al. 2022, ApJL, 940, L18